Available online at www.sciencedirect.com
ScienceDirect
Journal of Organometallic Chemistry 693 (2008) 874–893
Journal of Organometallic Chemistry
www.elsevier.com/locate/jorganchem

Some phosphinite complexes of Rh and Ir, their intramolecular reactivity and DFT calculations about their application in biphenyl metathesis

Klaus Ruhland *, Peter Gigler, Eberhardt Herdtweck

TU München, Lehrstuhl für Anorganische Chemie, Lichtenbergstr. 4, D-85748 Garching, Germany

Received 13 August 2007; received in revised form 26 September 2007; accepted 26 September 2007
Available online 18 October 2007

Abstract

Biphen(OPR_2) (with R: Ph, iPr, Cy) is reacted with $[Rh(COE)_2Cl]_2$. The corresponding μ-chloro-bridged dimers are received. An X-ray analysis of $[Biphen(OPCy_2)RhCl]_2$ is included. This compound shows a dynamic behaviour in solution, ascribed to a monomer/dimer equilibrium. The difference of the Biphen ligands to Milsteins PCP pincer-type ligand is shown. A catalytic cycle for biphenyl metathesis containing the coupling of oxidative addition and reductive elimination of the bridging C–C single bond in the biphenyl fragment using $Rh^{I/III}$ complexes and the concept of chelating assistance was calculated using DFT (B3PW91/LANL2DZ). According to the calculations the activation energy of the oxidative addition is about 30 kcal/mol and for the reductive elimination about 19 kcal/mol. The fac–Rh^{III} complex is by far the most stable compound, but the formation of it is kinetically strongly disfavoured. Pre-catalysts (COD)M(Ph-*O*-PR_2) (M: Rh, Ir) were synthesized by pre-coordinating the phosphinite to the metal (X-ray structures of four such compounds included) followed by treatment with 2 equiv. of sec. BuLi (X-ray structures of two such compounds included). In case of Ir this synthesis is complicated by C–H activation (X-ray structure of (COD)Ir(H)(Cl)(2-Br-phenyl-*O*-(diisopropylphosphinite)) included) and fast oxidative addition of the Ph-C–Halide bond. For (COD)Ir(H)(Cl)(2-phenyl-*O*-(diisopropylphosphinite)) the C–H activation is reversible and thermodynamic parameters for the ring closure reaction were determined by VT-NMR measurement ($\Delta H = -21.1 \pm 0.5$ kJ/mol, $\Delta S = -62.8 \pm 1.7$ J/(mol K)). The pre-catalysts were reacted with Biphen(OPR_2) to enter the calculated catalytic cycle. With Rh as center metal this reaction works out cleanly to give new complexes with the three P-atoms coordinated to one Rh center. No hemi-labile character was found for these P-donors even at 105 °C in toluene. If (COD)Rh(2-phenyl-*O*-(diisopropylphosphinite)) is reacted with 2 equiv. of 2-iodo-phenyl-*O*-(diisopropylphosphinite) oxidative addition of one C–Iodo bond is observed and the corresponding mer–Rh^{III} complex is received. Upon treatment with 2 equiv. of sec. BuLi the resulting product is(Biphen($OPiPr_2$))Rh^{I}(2-phenyl-*O*-(diisopropylphosphinite)) rather than mer–Rh^{III}(2-phenyl-*O*-(diisopropylphosphinite))$_3$. Reaction of $[Rh(COD)Cl]_2$ with 3 equiv. of 2-bromo-phenyl-*O*-(diphenylphosphinite) shows a fast scrambling of the chlorine into all possible *ortho* positions of the phenolate rings in the final Rh^{III} reaction product.

Keywords: Group 9 complexes; Metathesis

1. Introduction

C–C single bond metathesis of alkanes has been successfully performed using immobilized group-5 and group-6 catalysts by the group of Basset [1]. Mechanistic studies of this group show that the actual pathway of the reaction is not via the cleavage of a $C(sp^3)$–$C(sp^3)$ single bond but rather by a combination of C–H activation, α/β-H elimination, olefin metathesis and insertion processes. This reaction, although very important for oil chemistry in which the molecules contain a lot of C–H bonds connected to the C–C single bond under focus, cannot be transferred to a possible metathesis between biphenyl fragments.

* Corresponding author. Tel.: +49 89 289 13096; fax: +49 89 289 13473.
E-mail address: klaus.ruhland@ch.tum.de (K. Ruhland).

0022-328X/$ - see front matter © 2007 Elsevier B.V. All rights reserved.
doi:10.1016/j.jorganchem.2007.09.035

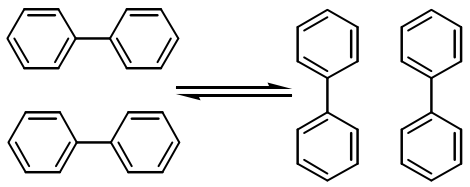

Scheme 1.

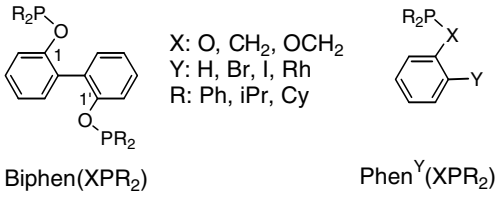

Scheme 2.

Those are components of coal and lignin chemistry, two sources for basic chemicals that might become more important in the future. If in analogy to alkane metathesis biphenyl molecular fragments are to be reorganized according to a metathesis reaction, the bridging C–C single bond must be broken meanwhile and reformed afterwards (Scheme 1).

We call this type of new reaction biphenyl metathesis. In spite of the fact that for late transition metals in low oxidation state (as for instance Ir^{I}) the oxidative addition of the bridging $C(sp^2)$–$C(sp^2)$ single bond, forming two $C(sp^2)$–M bonds, is expected to be thermodynamically favourable [2] and the kinetic hindrance for it should be much less pronounced than for alkane $C(sp^3)$–$C(sp^3)$ single bonds, there is by now no precedence for the activation or cleavage of a non-strained biphenyl molecular fragment. The strained biphenylene, though, has been activated and cleaved by several groups [3]. On the other hand the through-breaking work of Milstein and coworkers [4] showed that it is possible to cleave an aryl(sp^2)-methyl(sp^3) single bond by group 9 metal complexes and it demonstrated that in specific cases this reaction is thermodynamically favoured if chelating assistance is applied.

2. The difference to Milstein's pincer-type ligands

In light of the fact that Crabtree and coworkers could cleave one of the strained bridging $C(sp^2)$–$C(sp^2)$ single bonds in biphenylene using $[Ir(COD)Cl]_2$ on the one hand and that Milstein and coworkers could cleave the

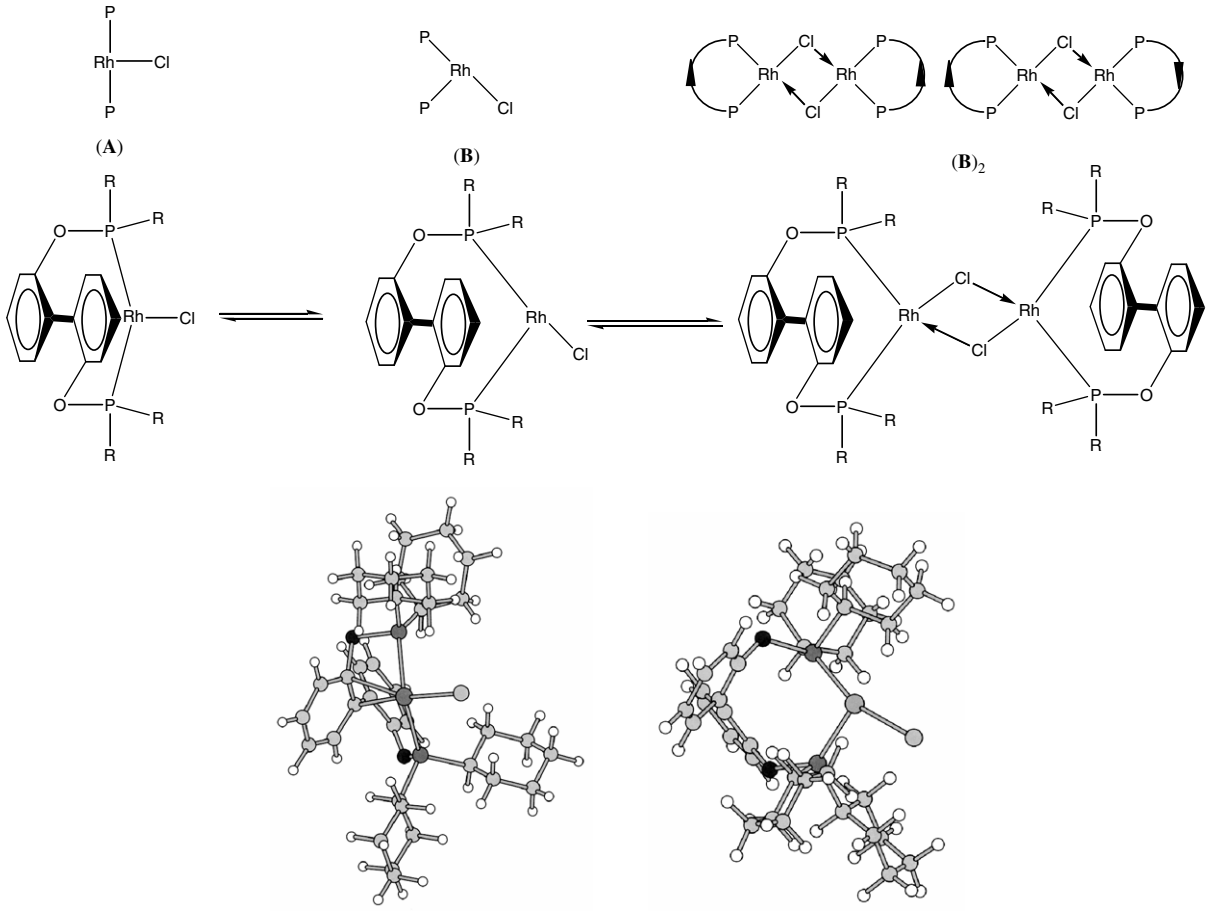

Scheme 3.

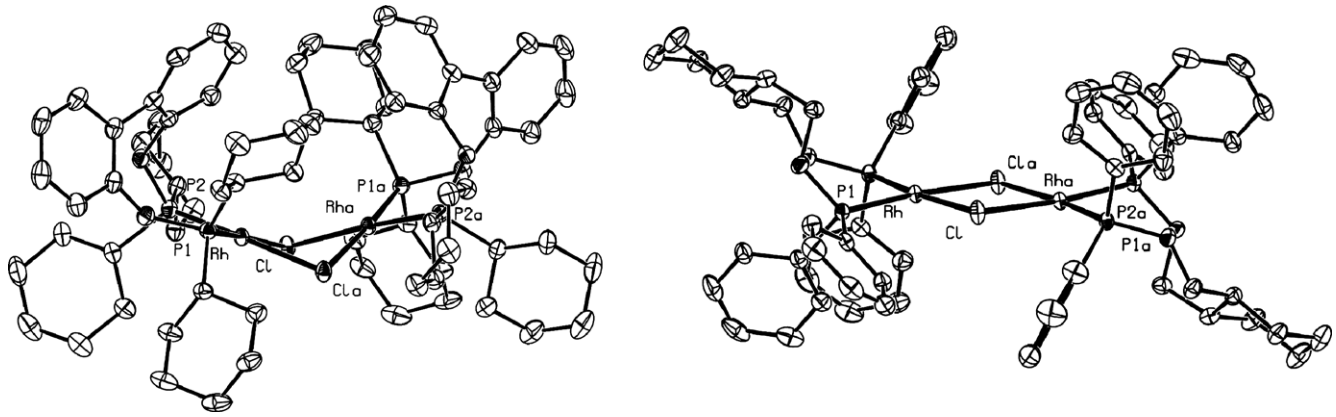

Fig. 1. Picture of a molecule in the solid state for [Biphen($OPCy_2$)RhCl]$_2$ and [Cy-1,2-CH_2($OPPh_2$)RhCl]$_2$. Hydrogens are omitted for clarity. Thermal ellipsoids are drawn at the 50% probability level.

non-strained C(sp^2)–C(sp^3) bond in their group-9 pincer-type complexes, we decided to apply a biphenyl ligand with phosphinites in 1 and 1′ position for chelating assistance to Rh^I (Scheme 2).

Thus, [Rh(COE)$_2$Cl]$_2$ (COE: Cyclooctene) was reacted with the Biphen(OPR_2) ligands (R: Ph, iPr, Cy) in benzene or dichloromethane at room temperature. ^{31}P NMR spectroscopy for [Biphen($OPPh_2$)RhCl]$_2$ showed two close sharp doublets ($\delta_1 = 140.5$ ppm, $^1J_{RhP} = 230.8$ Hz, $\delta_2 = 139.5$ ppm, $^1J_{RhP} = 231.6$ Hz) in the ratio 3.75:1, which we assign to the two possible configuration isomers of the μ-chloro-bridged dimer (B_2, Scheme 3). This is confirmed by the fact that the addition of 1 equiv. of PPh_3 per Rh gives [Biphen($OPPh_2$)](PPh_3)RhCl with only one set of signals for each of the three P atoms (O–P^1: 145.8 ppm ddd, $^1J_{RhP} = 216.0$ Hz $^2J_{PPcis} = 27.7$ Hz $^2J_{PPcis} = 35.7$ Hz; O–P^2: 131.2 ppm ddd $^1J_{RhP} = 176.4$ Hz $^2J_{PPcis} = 27.7$ Hz $^2J_{PPtrans} = 396.3$ Hz; PPh_3: 28.8 ppm ddd $^1J_{RhP} = 128.9$ Hz $^2J_{PPcis} = 35.7$ Hz $^2J_{PPtrans} = 396.3$ Hz). A similar result is obtained for Biphen($OPiPr_2$)RhCl ($\delta_1 = 179.7$ ppm, $\delta_2 = 179.3$ ppm, $^1J_{RhP} = 229.8$ Hz both, ratio 1:1). The reaction with PPh_3 results in this case in an equilibrium mixture between the two μ-chloro-bridged dimers and free PPh_3 on the one hand and the monomer with coordinated PPh_3 (ratio: dimer 2.1:monomer 1: free PPh_3 2.7 at room temperature; ratio does not change after 24 h; the P-atom peaks for the PPh_3-coordinated monomer are slightly broadened) on the other hand.

Table 1
Selected structural data for [Biphen($OPCy_2$)RhCl]$_2$ and [Cy-1,2-CH_2-($OPPh_2$)RhCl]$_2$

	[Biphen($OPCy_2$)RhCl]$_2$	[Cy-1,2-CH_2($OPPh_2$)RhCl]$_2$
Rh–P (Å)	2.1818(6)/2.1939(6)	2.1770(5)/2.1876(5)
Rh–Cl (Å)	2.4200(6)/2.4235(6)	2.4300(5)/2.4361(5)
Fold angle along Cl–Cl (°)	46.45	0
Cl–Rh–Cl (°)	79.10(2)	81.05(2)
P–Rh–P (°)	91.83(2)	89.43(2)

In case of Biphen($OPCy_2$)RhCl the signal at 179 ppm is decisively broadened at room temperature, indicating an equilibrium between monomer and dimer. PPh_3 is not permanently coordinated by this compound. In fact, the signal for PPh_3 in ^{31}P NMR spectroscopy appears at the same position as free PPh_3, but it is broadened. The peak of Biphen($OPCy_2$)RhCl at 179 ppm does not change significantly if PPh_3 is added. An X-ray structure of a molecule in the solid state for Biphen($OPCy_2$)RhCl showed only the μ-Cl-bridged dimeric structure (Scheme 3, Fig. 1, Table 1). A reference structure of a similar dimer with less sterically demanding ($OPPh_2$) donors and a somewhat different but still comparable backbone (–CH_2–Cy–CH_2–) is shown in Fig. 1. Selected structural data are listed in Table 1. According to this, the Rh–Cl bond length in $(\mathbf{B})_2^{Cy}$ (2.42 Å in $(\mathbf{B})_2^{Cy}$ and 2.43 Å in the reference structure) is not elongated in comparison to the reference structure, but the square planes of the two Rh centers are bent to each other in contrast to the reference structure in which all Rh, P and Cl atoms are in one and the same plane. The signals of the phenyl-carbons in ^{13}C NMR spectroscopy for Biphen($OPCy_2$)RhCl are broadened, too, at room temperature. A coupling of the bridging C-atoms to Rh or P that would be an indicator for an interaction between these carbons and the Rh center cannot be unequivocally determined (this coupling is expected to be smaller than 10 Hz). The synthesis of the ligand Biphen($OPtBu_2$), with the intention to support the dissociation of the dimer did not work out in our hands.

We calculated the structures for the two possible T-shape monomers (**A**) and (**B**) in Scheme 3 with R = Cy using DFT (B3PW91/LANL2DZ). Pictures of the calculated structures are included in Scheme 3. In structure (**A**) an interaction of the biphenyl fragment with the Rh center is found, but not as anticipated via the bridging C–C single bond. Only one of the bridging carbons takes part in this interaction; the second center in the biphenyl fragment is the carbon of the same phenyl ring that is connected to the oxo group. The C–C bond between these two carbons is elongated

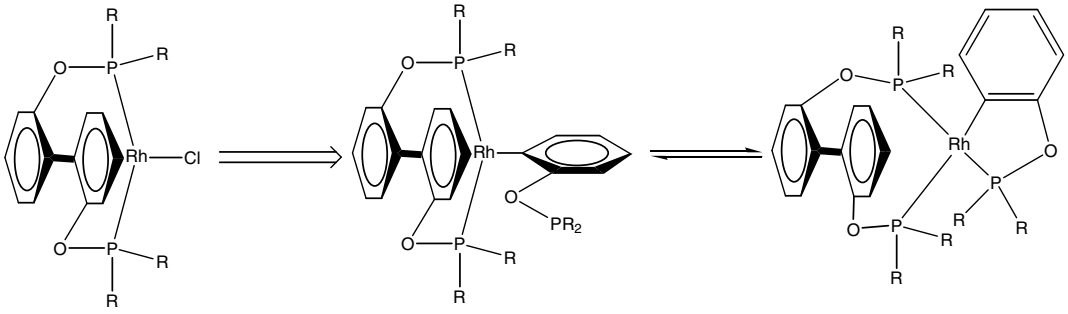

Scheme 4.

(d(C1–C2) = 1.44 Å, d(Rh–C1) = 2.46 Å, d(Rh–C2) = 2.65 Å). According to the calculations structure (**B**) is more stable than (**A**) by 6.7 kcal/mol. Thus, it must be concluded that even by forcing the dimer $(\mathbf{B})_2$ to dissociate through steric pressure, the T-shape isomer with the cis-connectivity of the P-donors is predominant, which in turn does not show interactions of the biphenyl fragment with the metal center. These first results point out that our substrate-ligand is more flexible than the unique Milstein-pincer-type ligand which does not allow for stable cis-complexes. To prevent the formation of a dimer and to prefer (**A**) over (**B**) we used the strategy shown in Scheme 4.

3. Results of the DFT calculations

On the base of a mechanism including a reversible oxidative addition/reductive elimination sequence via M^I/M^{III} metal centers we calculated the catalytic cycle shown in Scheme 5 for the case of R = Me in Scheme 4 using Density Functional Theory (B3PW91/LANL2DZ).

Some highlights concerning Scheme 5 and Fig. 2, which contains the energy profile of Scheme 5, are to be pointed out. First, the calculations indicate that there are two four-coordinate Rh^I structures of similar energy, one of them with square planar geometry **2a**. The other one is trigonal pyramidal **2a′**. A C–H-agostic interaction is found

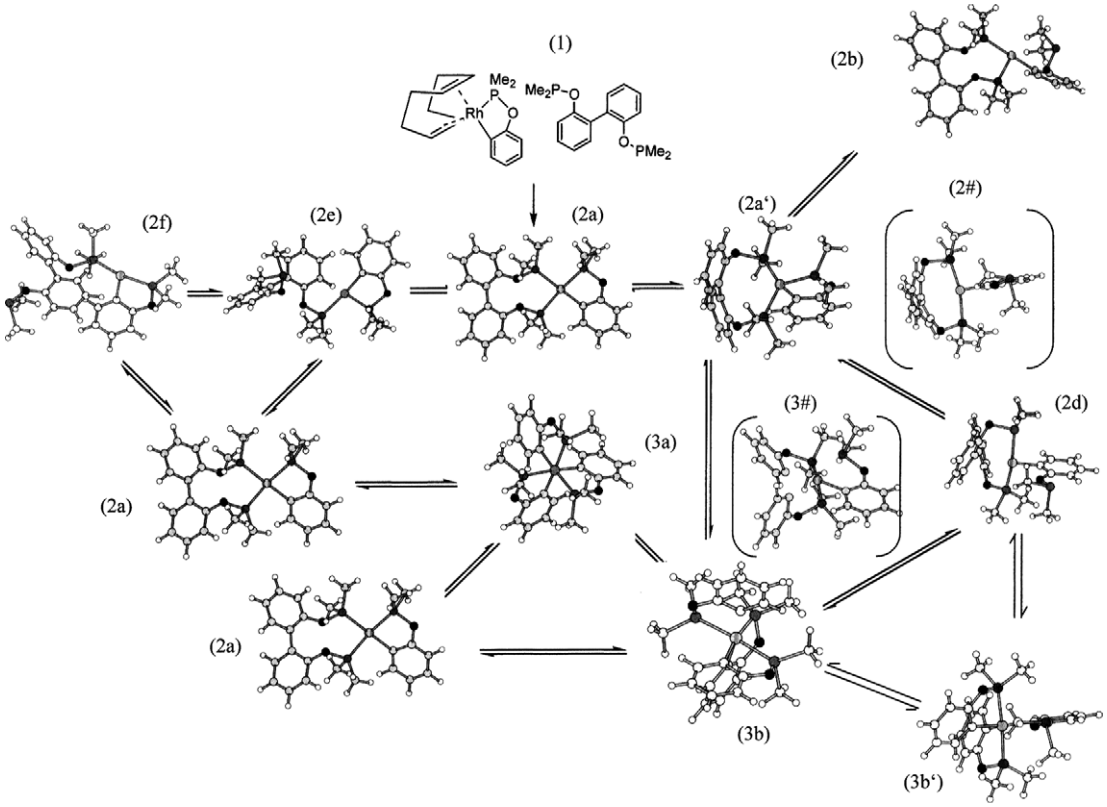

Scheme 5.

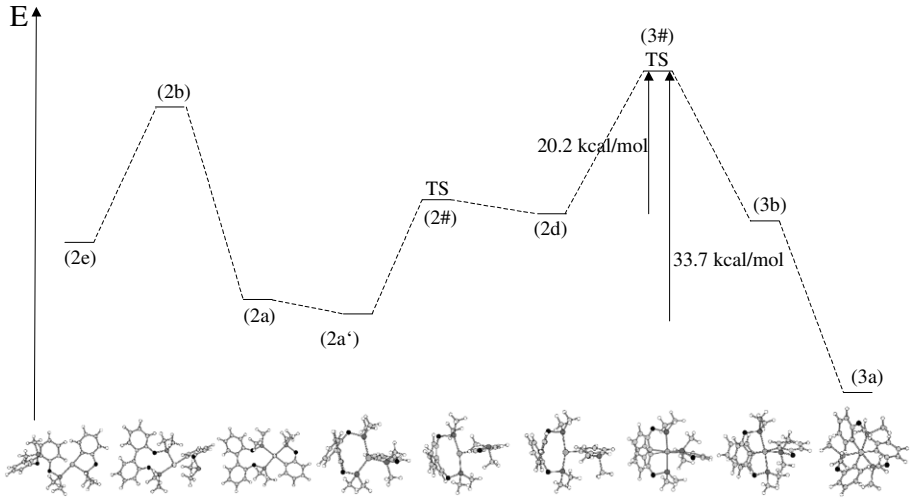

Fig. 2. Energy profile to Scheme 5.

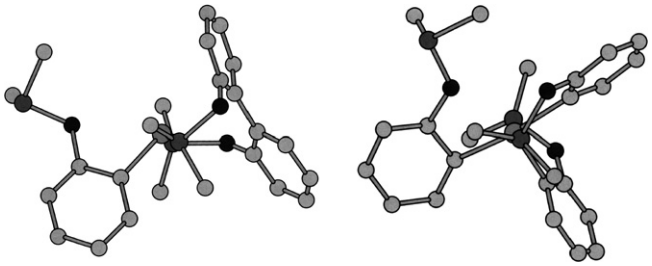

Fig. 3. Picture of the calculated structures of **2d** (left) and **3b′** (right), demonstrating the Rh–O interaction in **3b′** and the absence of such kind of interaction in **2d**.

for the T-shape complex **2e**. Interactions between the bridging oxo and the Rh center are found in (**3b′**) but not in **2d** (Fig. 3).

The fac–Rh^{III} complex **3a** is a thermodynamic sink in the system and would be a trap for the catalytic cycle, in contrast to the mer–Rh^{III} isomer **3b**. As jet, in this case we could not find a transition state (reasonable in energy) leading to the fac–Rh^{III} isomer, but we did find one leading to the mer–Rh^{III} complex (activation barrier for the oxidative addition: 33.7 kcal/mol).

In the transition state **3#** the distances of the two carbons that form new bonds to the metal center are not equal, and, thus, no completely concerted reaction takes place because of pseudo-Jahn-Teller effects in the d^8 starting geometry and the d^6 product geometry (Fig. 4).

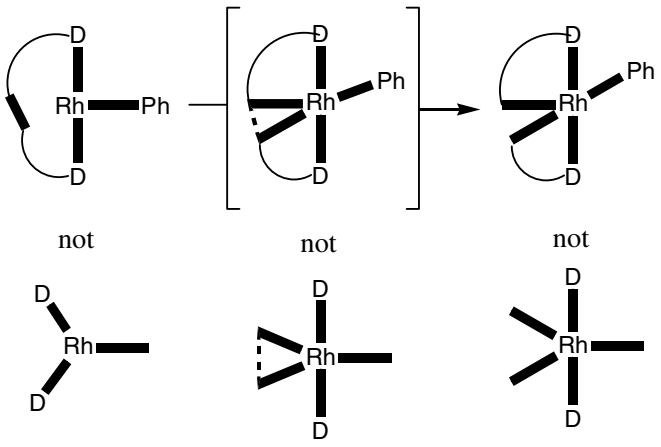

Fig. 4. Geometrical development during the oxidative addition to the d^8–Rh^I center with T-shape geometry which changes to a square pyramid d^6–Rh^{III} complex because of a pseudo-Jahn-Teller effect.

4. Synthesis of the pre-catalyst

The Rh-pre-catalysts in Scheme 5 can be synthesized by pre-coordination of the 2-bromo-phenylphosphinite (quantitative reaction) and successive treatment with 2 equiv. of sec. BuLi at −78 °C in diethylether (60–90% yield) (Scheme 6).

The 2-iodo derivative cannot be used because oxidative addition to Rh takes place and the resulting complexes decompose. Direct *ortho*-lithiation of the phosphinite without pre-coordination to Rh is not possible because the phosphinite rearranges to a 2-phosphino-phenolate. The use of *n*-BuLi instead of sec. BuLi in the second step leads to a considerable decrease in the yield. With PPh_2 donor hands the ring closure reaction in the second step did not always work. Fig. 5 shows pictures of a molecule in the solid state determined by X-ray analysis for (COD)Rh(Cl)($Phen^{Br}(OPiPr_2)$) (**1**), (COD)Rh($Phen^{Rh}$-$(OPiPr_2)$) (**2**) and for (COD)Rh($Phen^{Rh}(CH_2OPiPr_2)$) (**3**). Table 2 contains selected structural data. As can be seen in **2** the phenyl group plane is parallel to the square plane around the Rh while in **3** these planes are perpendicular to each other.

The synthesis of the analogous Ir-complexes is complicated by C–H activation and the more facile oxidative addition of a C–Halide bond by Ir in comparison to Rh (Scheme 7).

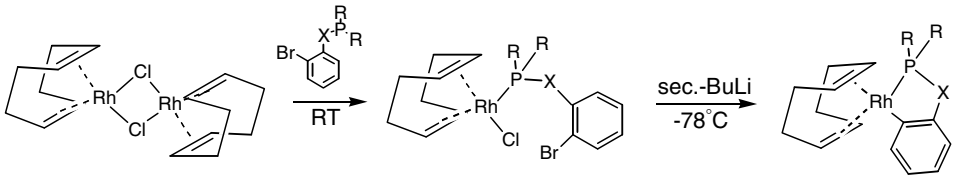

Scheme 6.

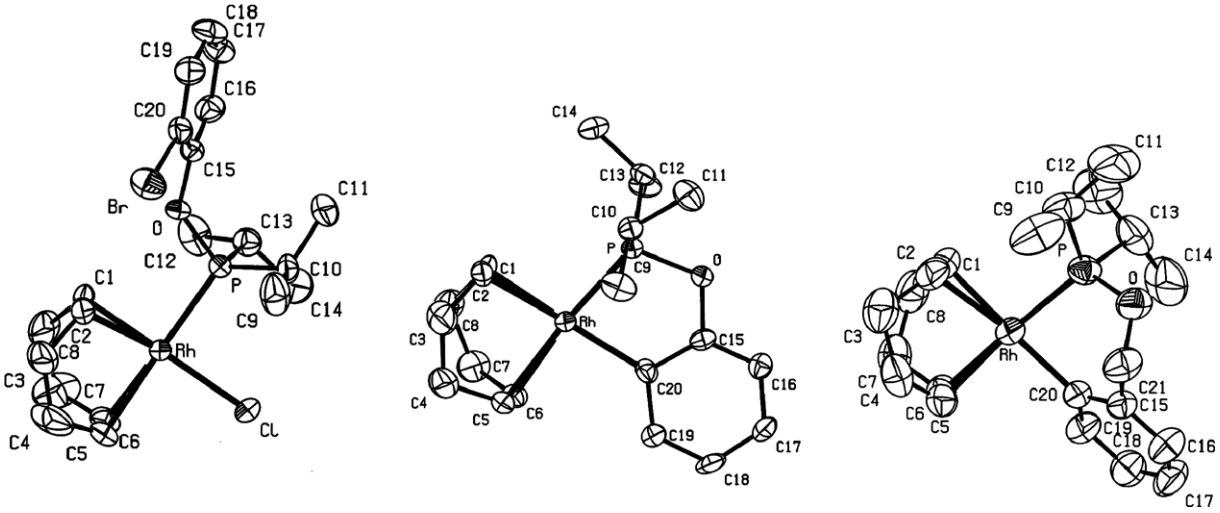

Fig. 5. Pictures of a molecule in the solid state for **1**, **2** and **3**. Hydrogens are omitted for clarity. Thermal ellipsoids are drawn at the 50% probability level.

If $[(COD)IrCl]_2$ is treated with $Phen^{Br}(OPiPr_2)$ exclusively *ortho*-C–H activation of the ligand is observed in contrast to the analogous Rh-complex. An X-ray analysis for compound **4** in Scheme 7 could be obtained. A picture of a molecule **4** in the solid state is shown in Fig. 6. Table 3 contains selected structural data.

If $[(COD)IrCl]_2$ is reacted with $Phen^{H}(OPiPr_2)$ the C–H activation process becomes reversible and both compounds **12** and **13** in Scheme 7 are observed. The thermodynamic data for the reaction of the C–H activation in this case were obtained by determining the amounts of both compounds at different temperatures using ^{31}P NMR spectroscopy ($\Delta H = -21.1 \pm 0.5$ kJ/mol and $\Delta S = -62.8 \pm 1.7$ J/(mol K) (**12** → **13**)). The equilibrium is reached almost instantaneously even at −30 °C in $CDCl_3$. Fig. 7 shows the Van't Hofft plot for this reaction.

The C–H activation can be prevented by substituting the *ortho*-H by fluorine. In this case the coordination takes place cleanly. An X-ray structure of a molecule in the solid state could be obtained for compound **5** in Scheme 7 and a picture of it is shown in Fig. 8 with some selected structural data summarized in Table 4 which are compared to the analogous Rh compound $\mathbf{5}^{Rh}$.

With compound **5** the ring closure reaction using sec. BuLi works without complications and compound **6** can be received in 88% yield. A second way to overcome the C–H activation is to extend the arm length of the added phosphinite ligand. If a CH_2-group is incorporated and $Phen^{Br}(CH_2OPiPr_2)$ is used, the addition of the ligand to $[(COD)IrCl]_2$ is possible without any C–H activation. A picture of a molecule in the solid state determined by X-ray analysis of the resulting complex **10** is shown in Fig. 8. Table 4 contains some selected structural data. We added bromoform to this reaction to check out whether

Table 2
Selected structural data for **1**, **2** and **3**

X: Cl or Ph(C)	1	2	3
Rh–P (Å)	2.2845(15)	2.2314(11)	2.261(2)
Rh–X (Å)	2.362(2)	2.070(4)	2.070(5)
C=C *trans* to X (Å)	1.397(11)	1.365(7)	1.362(10)
C=C *trans* to P (Å)	1.358(12)	1.355(7)	1.360(8)
Rh–C *trans* to X (Å)	2.1297(6)/ 2.127(6)	2.205(5)/ 2.188(5)	2.211(7)/ 2.249(6)
Rh–C *trans* to P (Å)	2.255(7)/ 2.239(7)	2.235(5)/ 2.239(4)	2.217(7)/ 2.252(6)
P–Rh–X (°)	89.37(6)	79.26(11)	84.9(2)

Table 3
Selected structural data for **4**

Ir–P (Å)	2.263(2)
Ir–Cl (Å)	2.516(2)
Ir–C(phenyl) (Å)	2.074(5)
C=C *trans* to phenyl (Å)	1.382(12)
C=C *trans* to P (Å)	1.376(9)
Ir–C *trans* to phenyl (Å)	2.304(7)/2.298(8)
Ir–C *trans* to P (Å)	2.309(6)/2.303(7)
P–Ir–Ph(C) (°)	80.70(15)

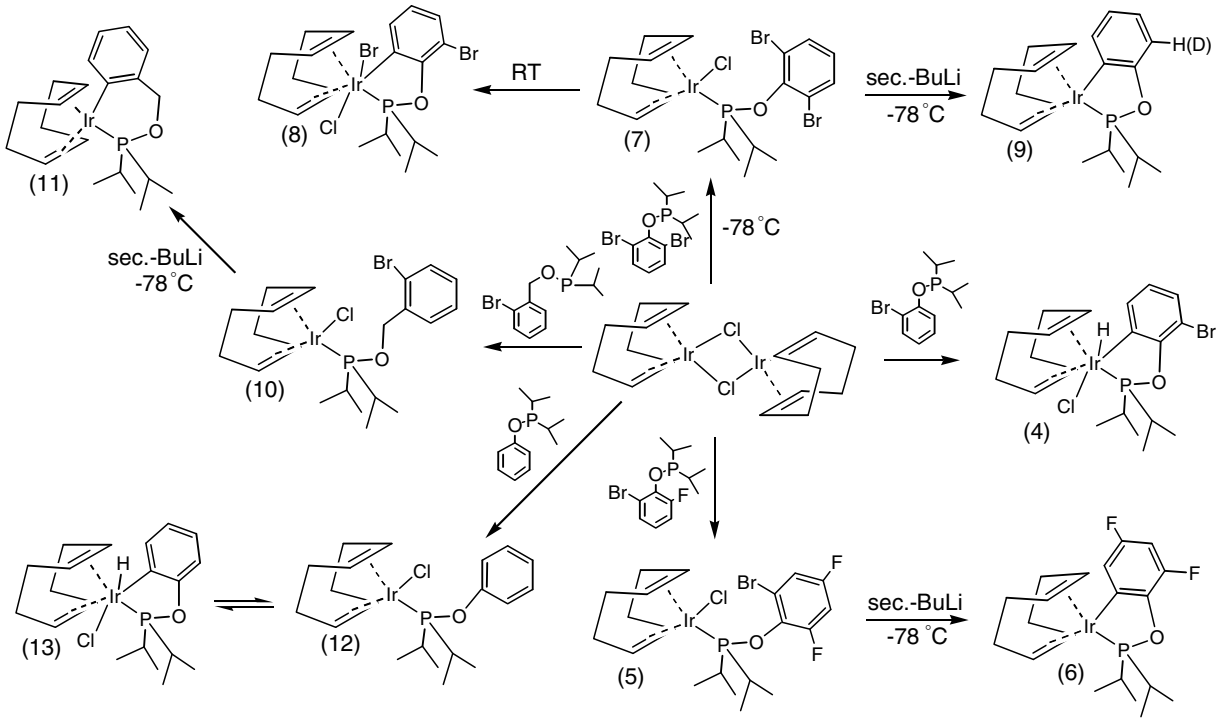

Scheme 7.

support for a fast reversible C–H-activation can be found by trapping the Ir–H, but no Ir–H/Br exchange was observed. The cyclization in the second step works (compound **11** in Scheme 7) in 68% yield. In the case of two bromine atoms in *ortho* position of the ligand's phenyl ring (2,6-Br-phenyl-*O*-(diisopropylphosphinite)) a slow oxidative addition is observed at room temperature (first order evaluation $k_{25\,^\circ C} = 0.0037\ min^{-1}$, product consists of four isomers (compound **8** in Scheme 7)). At 60 °C after 30 min the oxidative addition is quantitative. If the iPr-substituents at the phosphorous atom are exchanged by Ph-substituents 90 min are required for a quantitative oxidative addition at 60 °C. If the addition of the 2,6-dibromo ligands is performed at −78 °C followed by direct cyclization with 4 equiv. of sec. BuLi, compound **9** in Scheme 7 is received and if this reaction is quenched with D_2O instead of H_2O, 66% of the *ortho* protons are found to be deuterated.

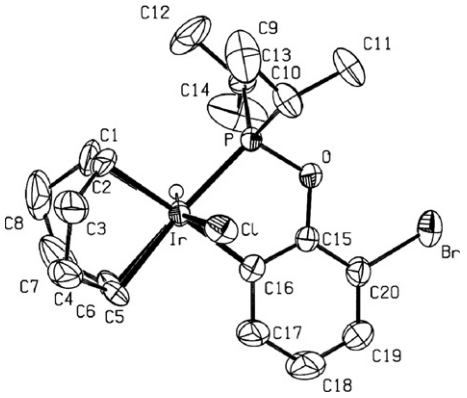

Fig. 6. Picture of a molecule in the solid state for **4**. Hydrogens are omitted for clarity. Thermal ellipsoids are drawn at the 50% probability level.

5. Entrance into the catalytic cycle

To enter the catalytic cycle of Scheme 5, **2** was reacted with Biphen($OPPh_2$). This reaction takes place quantitatively and within minutes (at most) at room temperature to give complex **14** (in contrast, the Ir complexes **6**, **9** and **11** do not readily exchange the COD even at elevated temperature). Free (and only free) COD is detected by ^1H NMR spectroscopy. In the presence of the new complex the 1,5-COD is isomerized within days at room temperature in toluene–d^8 to give 1,4-COD and finally 1,3-COD. The ^{31}P NMR spectrum shows three ddd groups of peaks for the new complex indicating that now three P-atoms are coordinated at one Rh center (Fig. 9).

The $^2J_{PP}$ coupling constants unequivocally prove a T-shape orientation of the three P atoms to each other (two ct couplings combined with one cc coupling). The values of the $^1J_{RhP}$ coupling constants (all of them are decisively larger than 100 Hz) support the oxidation state I for the Rh center, although this diagnostic criterion is not unequivocal. From these findings the calculated structure **2a**′ of Scheme 5 can be excluded since in this structure no T-shape geometry for the three P-atoms is found (the angle between the P-atoms is almost 120°). No line-broadening or other indicators of a dynamic behaviour could be

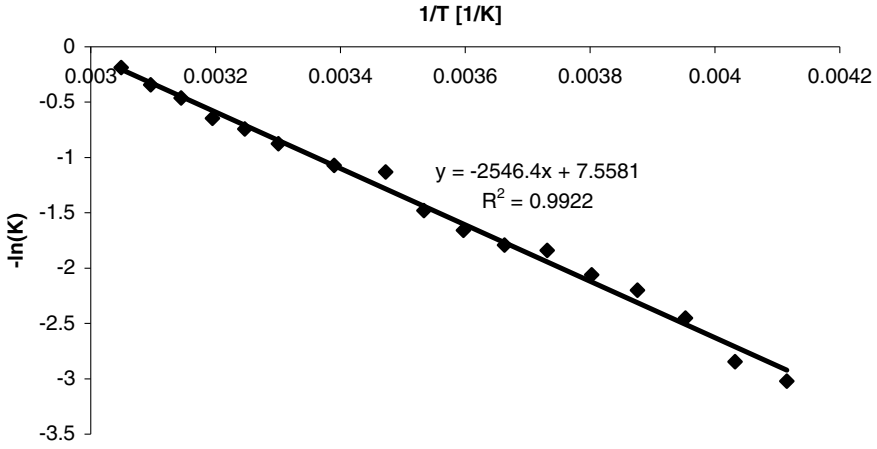

Fig. 7. Van't Hofft plot for the reaction **12** → **13**.

detected by ^{1}H or ^{31}P NMR spectroscopy up to 105 °C in toluene–d^8. Thus, no hemi-labile character is found for the ligand constellation of **14**. No hemi-labile behaviour is induced if the iPr-rests at the P donor in **14** are exchanged for Cy or if the spacer between the phenyl group and the P-donor is extended to CH_2–O (tBu rests can be introduced into the mono-phosphinite ligand by refluxing the phenol with $(tBu)_2PCl$ in acetonitrile for 10 days but the coordination of this ligand to $[Rh(COD)Cl]_2$ is not clean and leads to a mixture of products containing unreacted starting material as well as free COD). **14** can be synthesized alternatively by starting with $[Biphen(OPPh_2)RhCl]_2$ (although with decisively lower yield in the last step).

In light of the results collected with $[Biphen(OPiPr_2)RhCl]_2$ and PPh_3 we reacted **2** with $Biphen(OPiPr_2)$ (Fig. 10). The ligand exchange reaction takes place, although very slowly at room temperature. Even on heating to 60 °C the complete reaction takes 2 weeks. Raising the temperature above 60 °C leads to a decomposition of the complex indicated by a signal in ^{31}P NMR spectroscopy at about 50 ppm which appears as one single peak.

The coupling constants as well as the quite different chemical shifts of the three P atoms in **15** are listed in Fig. 11. The P atom with the signal at about 175 ppm shows the expected values for a simple T-shape structure (one $^{2}J_{pp}$c and one $^{2}J_{PP}$t coupling) in a Rh^{I} complex ($^{1}J_{RhP}$ coupling decisively larger than 100 Hz). In contrast, the other two P atoms show peculiarities that are not consistent with a T-shape geometry. The $^{2}J_{PP}$ coupling constant between them (100 Hz) points towards an P–Rh–P angle decisively larger than 90°. Also, the $^{1}J_{RhP}$ coupling constant of the signal at 118 ppm is unusually small for Rh^{I}. We propose therefore a distorted structure for **15** (similar to **2a**′ in Scheme 5 but not equal to it) rather than one showing a square planar geometry around Rh (Fig. 11).

This also explains the large differences in the chemical shifts of the three P atoms. As can be seen from Fig. 11 no evidence (through line broadening) for a hemi-labile behaviour is found in this compound (even at 105 °C in toluene–d^8).

To synthesize compounds **3** of Scheme 5 in order to get insight into the Rh^{III} chemistry of the anticipated catalytic

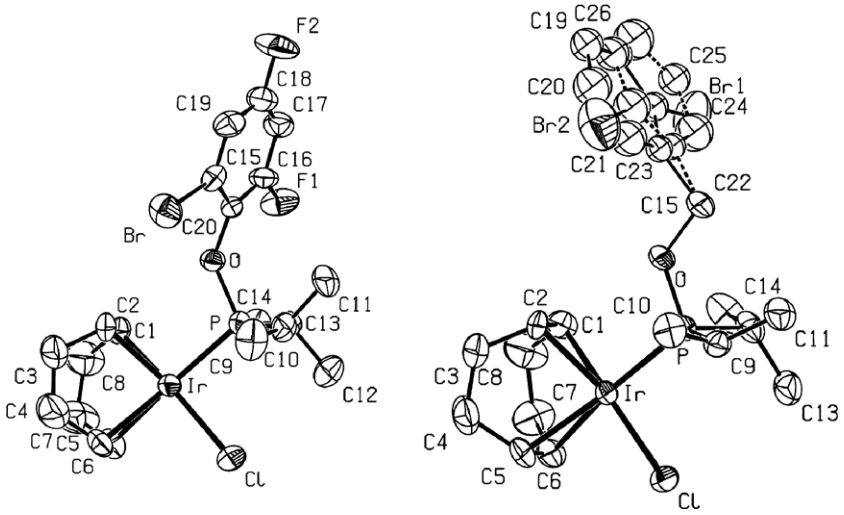

Fig. 8. Pictures of a molecule in the solid state for **5** and **10**. Hydrogens are omitted for clarity. Thermal ellipsoids are drawn at the 50% probability level.

Table 4
Selected structural data for **5**, $\mathbf{5}^{Rh}$ and **10**

M: Rh or Ir	**5**	$\mathbf{5}^{Rh}$	**10**
M–P (Å)	2.282(2)	2.282(2)	2.286(2)
M–Cl (Å)	2.360(2)	2.369(2)	2.359(2)
C=C *trans* to Cl (Å)	1.390(15)	1.371(12)	1.419(15)
C=C *trans* to P (Å)	1.366(15)	1.366(13)	1.365(15)
M–C *trans* to Cl (Å)	2.107(8)/ 2.123(9)	2.134(8)/ 2.122(6)	2.132(10)/ 2.113(9)
M–C *trans* to P (Å)	2.228(10)/ 2.195(10)	2.240(8)/ 2.240(8)	2.227(9)/ 2.202(8)
P–M–Cl (°)	90.62(7)	89.64(6)	90.87(8)

cycle we used the strategy shown in Fig. 10, **pathway** (**B**). Heating **2** in toluene–d^8 at 100 °C for 5 h with 2 equiv. of $Phen^{Iodo}(OPiPr_2)$ results in the meridional Rh^{III} compound **16**. The Rh^{III} character is proven by the small $^1J_{RhP}$ constants found (Fig. 12). The meridional geometry can be unequivocally deduced by the $^2J_{PP}$ coupling constants. If compound **16** is reacted with 2 equiv. of sec. BuLi the isolated product is compound **15** and not the mer–Rh^{III} complex. This is in accordance with the results of the calculations presented in Fig. 3, which indicate that the mer–Rh^{III} is much less stable than **15**. Also the activation

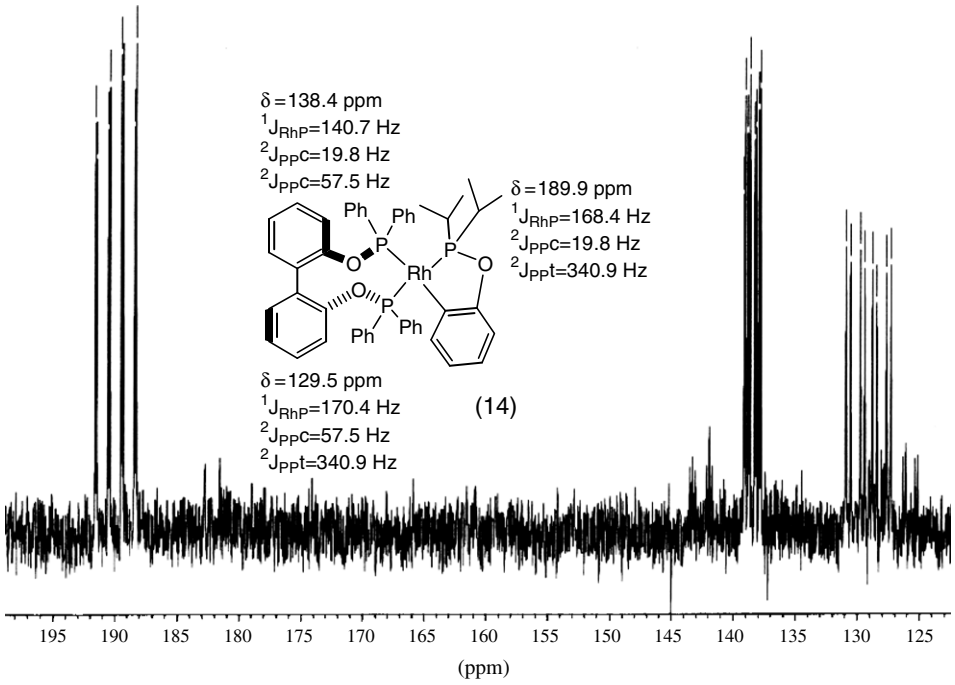

Fig. 9. Excerpt of the ^{31}P NMR spectrum for the product of the reaction of **2** with Biphen($OPPh_2$) showing the three groups of signals for the three P atoms bound to Rh.

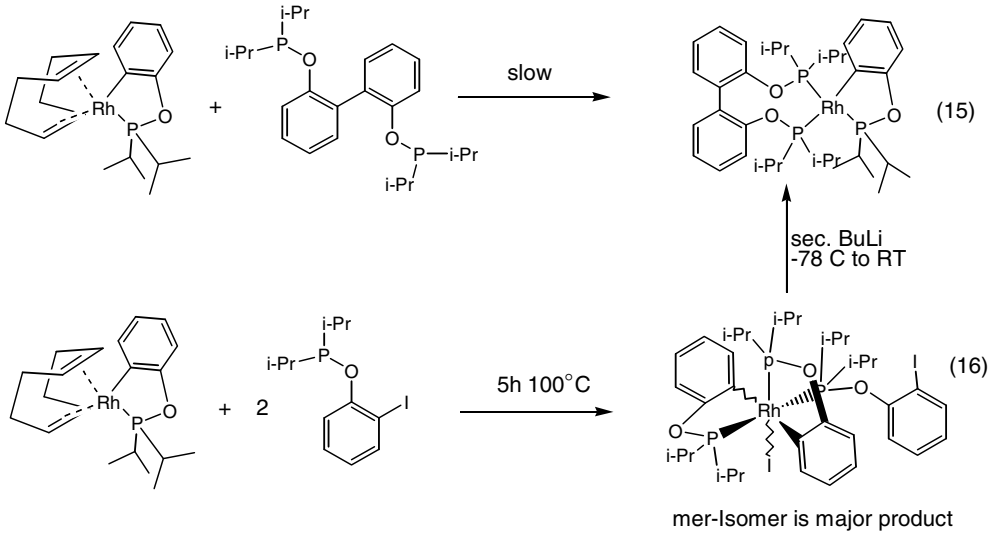

Fig. 10. Reactions involving ligands with R = iPr exclusively.

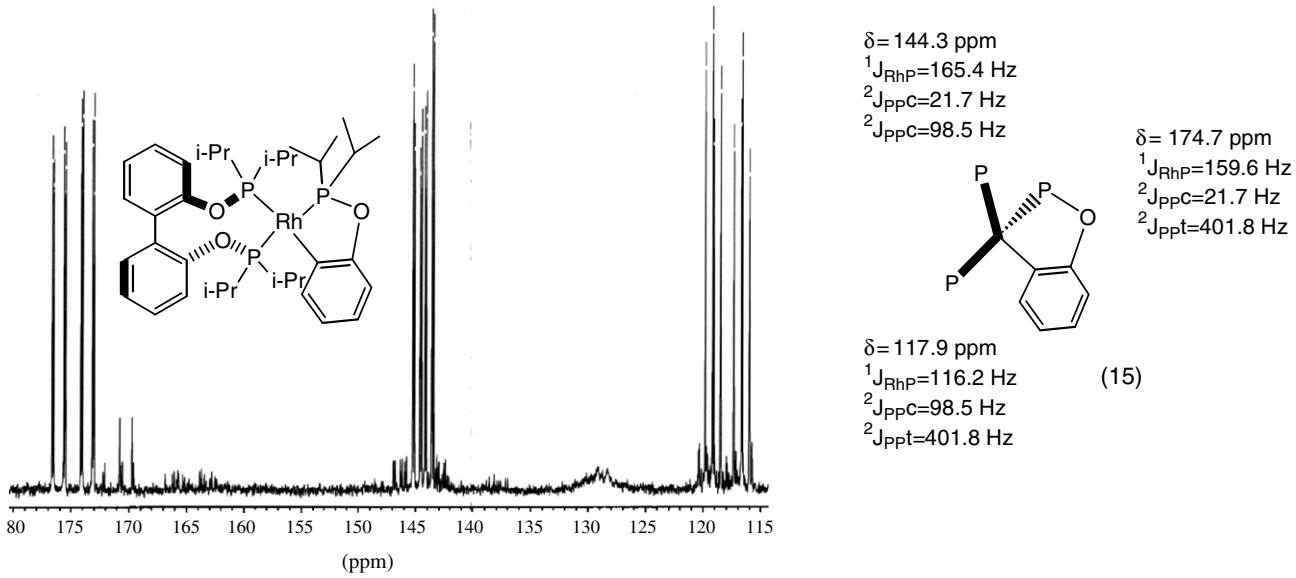

Fig. 11. Excerpt of the ^{31}P NMR spectrum of **15**.

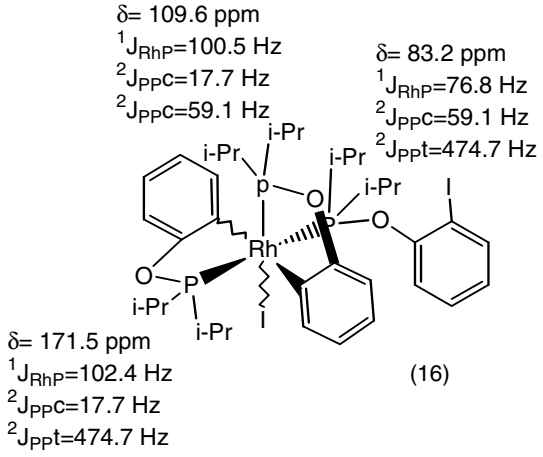

Fig. 12. Data extracted from the ^{31}P NMR spectrum of **16**.

barrier of about 20 kcal/mol is in accordance with the reductive elimination taking place at room temperature (calculated k about 0.1 s^{-1} for Methyl groups at the phosphorous). To prove that **15** is static rather than (degenerate) dynamic, we synthesized **15** with F atoms in 2- and 4-position of the *ortho*-metallated phenyl group and in a sec. experiment with Cy rests instead of iPr at the P atom connected to the *ortho*-metallated phenyl group via the oxo. In both cases only one single isomer was detected by ^{31}P NMR as well as ^{19}F NMR spectroscopy.

6. Experimental support for the proposed principle mechanism

That the equilibrium system used for the calculation in Scheme 5 is a reasonable pathway, can be supported by the following experimental finding: if $[Rh(COD)Cl]_2$ is reacted with 3 equiv. of $Phen^{Br}(OPPh_2)$ at room temperature in $CDCl_3$ or toluene–d^8 the instantaneous formation of four very similar isomers is observed by ^{31}P NMR spectroscopy. A VT NMR study in toluene–d^8, allowing the reaction to start at −80 °C, proves that in the first place $Rh^I(Phen^{Br}(OPPh_2))_3Cl$ is formed ($\delta_1 = 133.9$ ppm, $^1J_{P1Rh} = 201.9$ Hz; $\delta_2 = 123.9$ ppm, $^1J_{P2Rh} = 162.9$ Hz, $^2J_{PP(cis)} = 36.7$ Hz) which transforms extremely fast into four very similar meridional Rh^{III} isomers **17** at temperatures above −40 °C ($^1J_{P1Rh} = 144.7$ Hz, $^1J_{P2Rh} = 109.0$ Hz, $^2J_{PP(cis)} = 21$ Hz, for all four isomers the same, ratio 1:1:0.65:0.73, excess ligand does not change the ratio) (Fig. 13). No peaks are found in the negative area up to −40 ppm in the proton NMR spectrum. Re-cooling the sample from room temperature to −50 °C does not change the ratio or shape of the peaks.

An X-ray structure of a molecule in the solid state reveals the nature of the reaction product (Fig. 14).

A scrambling of the chlorines into the *ortho* positions of the phenyl rings is unequivocally found. The finding can be explained by a sequence of an oxidative addition of a C–Br or a C–H bond followed by a reductive elimination of a C–Cl bond and another irreversible oxidative addition of a C–Br bond. Considering just the elemental steps, this is similar to the behaviour shown in Scheme 5 for the biphenyl metathesis. We admit that in spite of this analogy there is still a considerable difference between the two cases. The oxidative addition of the bridging phenyl C–Ph single bond in a biphenyl fragment is much more challenging than the oxidative addition of a phenyl C–Br, C–H or C–Cl bond. Also, according to the X-ray analysis there is a discrepancy between the expected and found amounts of Br (3 vs. 2.5) and Cl (1 vs. 2.2) (the reaction was done in benzene–d^6 and the crystallization in benzene–d^6/pentane) which we cannot explain at the moment. That we are not too far away from the truth, can be further supported by the behaviour of $Rh^I(Phen^H(OPiPr_2))_3Cl$. This compound is stable at room temperature ($\delta_1 = 137.4$ ppm,

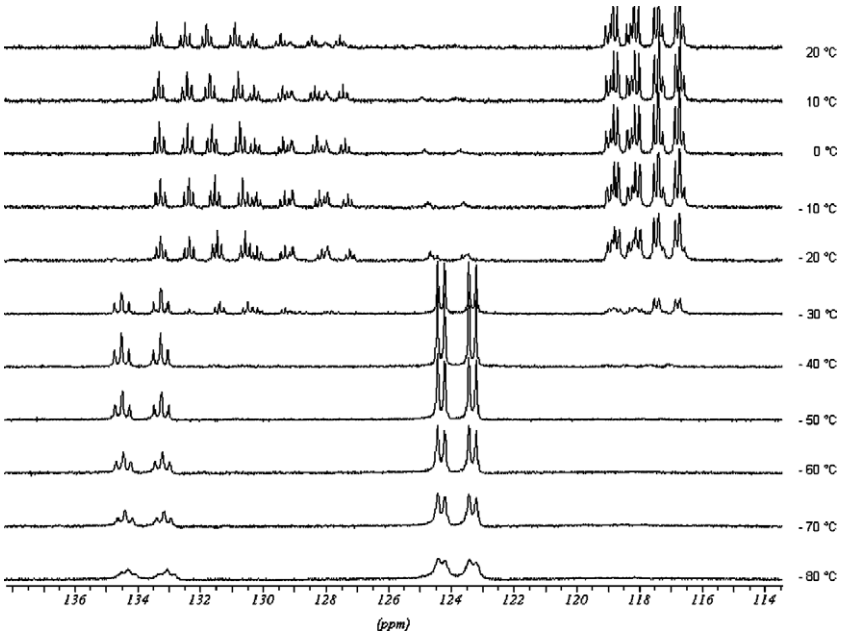

Fig. 13. Excerpt of the ^{31}P NMR spectrum at different temperatures for the reaction of $[Rh(COD)Cl]_2$ with $Phen^{Br}(OPPh_2)$.

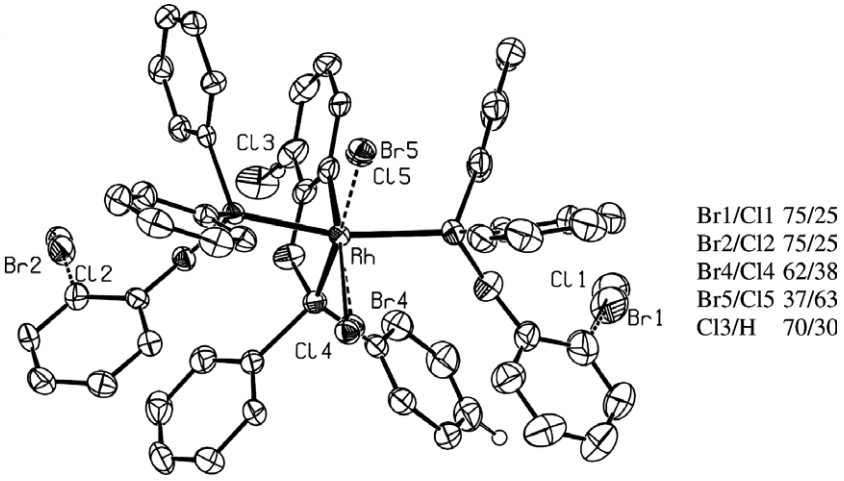

Fig. 14. Picture of a molecule in the solid state for **17**. Hydrogens are omitted for clarity. Thermal ellipsoids are drawn at the 50% probability level. On the right-hand side are listed the occupancy ratios over the five positions.

$^1J_{P1Rh} = 213.4$ Hz, $\delta_2 = 128.5$ ppm, $^1J_{P2Rh} = 162.9$ Hz, $^2J_{PP} = 36.7$ Hz). No peaks are found in the proton spectrum in the negative area up to −40 ppm. But by addition of about 3 equiv. of bromoform two products very similar to **17** are detected by ^{31}P NMR spectroscopy, CH_2Br_2 is observed and another Rh^I complex similar to the starting compound is formed. We explain this finding as shown in Scheme 8.

7. Conclusion

The *calculated* results presented in this paper indicate that biphenyl metathesis as a yet unknown reaction seems in general to be possible, although we admit that an *experimental* proof is not provided in this paper. The proposed mechanism involving an oxidative addition and a reductive elimination of the bridging C–C single bond in a biphenyl fragment at $Rh^{I/III}$ complexes bearing a phenyl ligand could be made plausible by DFT calculations. The introducing synthetic work presented in this paper shows that the proposed (pre)catalysts are available. The calculated activation barrier of 30 kcal/mol for the cleavage of the bridging C–C single bond is still rather high, though. At least, for a phenyl C–Halide rather than a phenyl C–Ph bond the mechanism via oxidative addition and reductive elimination using Rh^I complexes with phosphinite

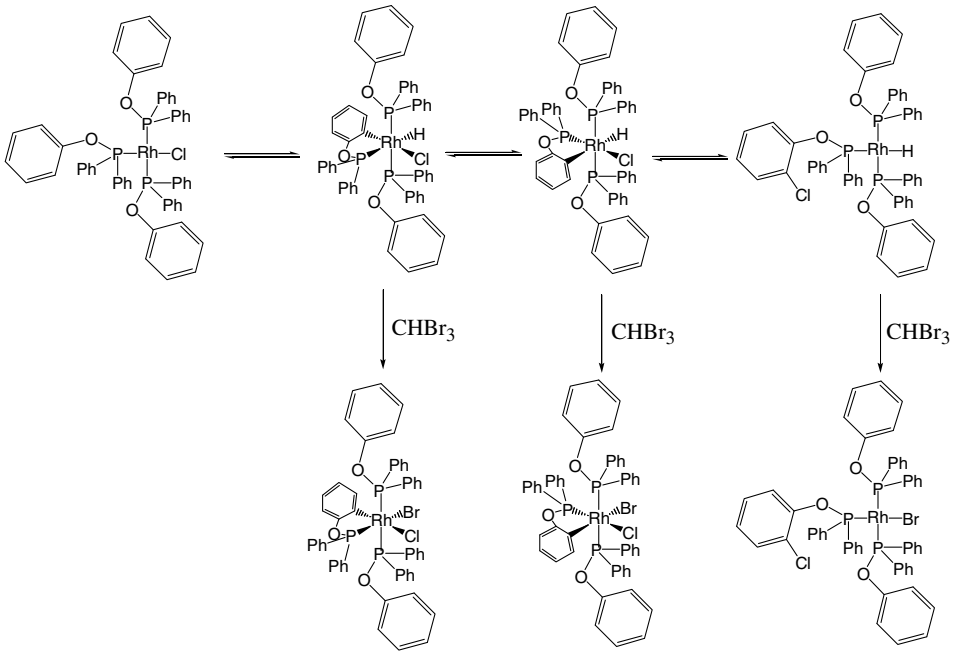

Scheme 8.

ligands could be experimentally confirmed. But these two processes (C–Halide vs. C–Ph) are admittedly still considerably different.

8. Experimental section

Manipulations and experiments were performed under an argon atmosphere using standard Schlenk techniques and/or in an argon-filled glove-box if not mentioned otherwise. Diethylether, pentane, acetonitrile, dichloromethane, toluene and THF were dried and degassed using a two-column-drying system (MBraun) and stored under an argon atmosphere over molecular sieves. $CDCl_3$ and toluene–d^8 were stored under argon over molecular sieves. $RhCl_3$ * Hydrate, $IrCl_3$ * Hydrate, $(NH_4)_2IrCl_6$ and chlorodicyclohexylphosphane were purchased from Strem Chemicals and used without further manipulation. 1Z,5Z-cyclooctadiene (COD), cyclooctene (COE), chlorodiphenylphosphane and 2,2′-dihydroxbiphenyl were purchased from VWR internatioanl, chlorodiisopropylphosphane, 2-bromo-phenol, 2,6-dibromophenol, 2-iodo-phenol, 2-bromo-benzylic alcohol, 2-bromo-4,6-difluorophenol were purchased from Aldrich and sec. Butyl-Lithium from Acros Organics and they were all used without further purification. $[(COD)RhCl]_2$, $[(COE)_2RhCl]_2$, $[(COD)IrCl]_2$ and $[(COE)_2IrCl]_2$ were synthesized according to the literature [5].

The NMR measurement was performed on a Bruker AMX400. ^1H NMR (7.24 ppm, 400 MHz) and ^{13}C NMR (77.0 ppm, 100 MHz) spectra were referred to the $CDCl_3$/$CHCl_3$ resonances, ^{31}P NMR (161 MHz) to 85% H_3PO_4 as external standard, ^{19}F NMR (376 MHz) to hexafluorobenzene (−162.9 ppm) as external standard.

9. Ligand synthesis

9.1. General procedure

0.31 mL (0.509 g; 2.94 mmol; 1 equiv.) of 2-bromo-phenol are dissolved in 10 mL acetonitrile and 0.82 mL (0.596 g; 5.89 mmol; 2 equiv.) of triethylamine are added. Then 0.52 mL (0.497 g, 3.27 mmol; 1.1 equiv.) of chlorodiisopropylphosphane are slowly added. A white precipitate forms. The suspension is stirred for 1.5 h at room temperature. Then 40 mL of pentane are added and it is stirred for another 20 min at room temperature. After this the pentane phase is separated via canula and the pentane is removed in vacuo to yield a slightly yellow oil (yield: 68%).

9.1.1. 2-Br-phenyl-O-(dicyclohexylphosphinite)

^1H NMR ($CDCl_3$, ppm): 1.2–2.0 (22H, unres. m, Cy-H), 6.80 (1H, t $^3J_{HH} = 7.2$ Hz), 7.19 (1H, t $^3J_{HH} = 7.4$ Hz), 7.25 (1H, d $^3J_{HH} = 7.2$ Hz), 7.48 (1H, d $^3J_{HH} = 7.4$ Hz); ^{13}C NMR ($CDCl_3$, ppm): 26.32 (s), 26.67 (d $J_{CP} = 7.3$ Hz), 26.80 (s), 26.90 (d $J_{CP} = 6.6$ Hz), 27.65 (d $J_{CP} = 17.6$ Hz), 37.85 (d $J_{CP} = 17.6$ Hz), 113.71 (s), 118.50 (d $J_{CP} = 21.2$ Hz), 122.23 (s), 128.18 (s), 133.06 (s), 155.96 (d, $J_{CP} = 10.2$ Hz); ^{31}P NMR ($CDCl_3$, ppm): 148.7; EA Calc. for $C_{18}H_{26}OPBr$: C, 58.55; H, 7.10; P, 8.39; Br, 21.64. Found: C, 58.77, 7.35; P, 8.22; Br, 21.12%.

9.1.2. 2-Br-phenyl-O-(diphenylphosphinite)

^1H NMR ($CDCl_3$, ppm): 6.90 (1H, t $^3J_{HH} = 7.4$ Hz), 7.18 (2H, t and d overlapp), 7.39 (6H, m), 7.53 (1H, d $^3J_{HH} = 7.4$ Hz), 7.67 (4H, m); ^{13}C NMR ($CDCl_3$, ppm): 114.67 (s), 119.0 (d $J_{CP} = 17.6$ Hz), 123.57 (s), 128.39 (s), 128.50 (d $J_{CP} = 7.3$ Hz), 129.89 (s), 130.55 (d $J_{CP} = 23.4$ Hz), 133.36

(s), 140.51 (d $J_{CP} = 17.6$ Hz), 153.90 (d $J_{CP} = 10.2$ Hz); ^{31}P NMR ($CDCl_3$, ppm): 113.1; EA Calc. for $C_{18}H_{14}OPBr$: C, 60.53; H, 3.95; P, 8.67. Found: C, 60.25; H, 4.04; P, 8.85%.

9.1.3. 2-Br-benzyl-O-(diisopropylphosphinite)

^{1}H NMR ($CDCl_3$, ppm): 0.94 (3H, d $^3J_{HH} = 7.4$ Hz), 0.98 (3H, d $^3J_{HH} = 7.4$ Hz), 1.04 (3H, d $^3J_{HH} = 7.4$ Hz), 1 (3H, d $^3J_{HH} = 7.4$ Hz), 1.71 (2H, hept $^3J_{HH} = 7.4$ Hz), 4.73 (2H, d $J_{PH} = 7.4$ Hz), 7.06 (1H, t $^3J_{HH} = 7.4$ Hz), 7.23 (1H, t $^3J_{HH} = 7.4$ Hz), 7.43 (2H, d $^3J_{HH} = 7.4$ Hz); ^{13}C NMR ($CDCl_3$, ppm): 17.25 (d $J_{CP} = 19.5$ Hz), 17.83 (d $J_{CP} = 17.6$ Hz), 28.28 (s), 73.48 (d $J_{CP} = 15.5$ Hz), 127.89 (s), 129.55 (d $J_{CP} = 20.4$ Hz), 133.36 (s), 138.51 (d $J_{CP} = 10.6$ Hz); ^{31}P NMR ($CDCl_3$, ppm): 155.6.

9.1.4. 2,6-Dibrom-phenyl-O-(diisopropylphosphinite)

^{1}H NMR ($CDCl_3$, ppm): 1.14 (6H, d $^3J_{HH} = 6.1$ Hz), 1.18 (6H, d $^3J_{HH} = 6.1$ Hz), 2.17 (2H, hept $^3J_{HH} = 6.1$ Hz), 6.73 (1H, t $^3J_{HH} = 7.3$ Hz), 7.45 (2H, d $^3J_{HH} = 7.3$ Hz); ^{13}C NMR ($CDCl_3$, ppm): 17.53 (d $J_{CP} = 20.5$ Hz), 17.65 (d $J_{CP} = 18.3$ Hz), 29.95 (d $J_{CP} = 22.7$ Hz), 116.79 (d $J_{CP} = 2.2$ Hz), 124.43 (s), 133.17 (s), 151.98 (s); ^{31}P NMR ($CDCl_3$, ppm): 171.22; EA Calc. for $C_{12}H_{17}OPBr_2$: C, 39.16; H, 4.66; P, 8.42. Found: C, 39.08; H, 4.04; P, 8.85%.

9.1.5. 2-I-phenyl-O-(diisopropylphosphinite)

^{1}H NMR ($CDCl_3$, ppm): 1.01 (3H, d $^3J_{HH} = 7.4$ Hz), 1.07 (3H, d $^3J_{HH} = 7.4$ Hz), 1.11 (3H, d $^3J_{HH} = 7.4$ Hz), 1.15 (3H, d $^3J_{HH} = 7.4$ Hz), 1.91 (2H, hept $^3J_{HH} = 7.4$ Hz), 6.60 (1H, t $^3J_{HH} = 7.4$ Hz), 7.27 (2H, d and t overlapp), 7.62 (1H, d $^3J_{HH} = 7.4$ Hz); ^{13}C NMR ($CDCl_3$, ppm): 17.18 (d $J_{CP} = 8.0$ Hz), 17.57 (d $J_{CP} = 19.8$ Hz), 28.17 (d $J_{CP} = 17.6$ Hz), 88.5 (s), 117.00 (d $J_{CP} = 22.0$ Hz), 122.84 (s), 129.6 (s), 139.20 (s), 157.90 (d $J_{CP} = 8.8$ Hz); ^{31}P NMR ($CDCl_3$, ppm): 153.5; EA Calc. for $C_{12}H_{18}OPI$: C: 42.88; H, 5.40; P, 9.21. Found: C, 52.53; H, 5.21; P, 9.54%.

9.1.6. 2-Br-phenyl-O-(diisopropylphosphinite)

^{1}H NMR ($CDCl_3$, ppm): 0.95 (6H, dd $^3J_{HH} = 7.4$ Hz $^3J_{PH} = 15.9$ Hz), 1.15 (6H, dd $^3J_{HH} = 7.4$ Hz $^3J_{PH} = 11.0$ Hz), 1.79 (2H, dhept $^3J_{HH} = 7.4$ Hz $^3J_{PH} = 15.9$ Hz), 6.46 (1H, t $^3J_{HH} = 7.4$ Hz), 7.38 (2H, d $^3J_{HH} = 9.8$ Hz), 7.43 (1H, dd $^3J_{HH} = 8.6$ Hz $^4J_{HH} = 3.7$ Hz); ^{13}C NMR ($CDCl_3$, ppm): 17.08 (d $J_{CP} = 12.9$ Hz), 17.53 (d $J_{CP} = 30.6$ Hz), 28.52 (d $J_{CP} = 30.6$ Hz), 114.18 (s), 118.58 (s), 118.79 (s), 122.65 (s), 133.57 (s), 156.25 (d $J_{CP} = 8.8$ Hz); ^{31}P NMR ($CDCl_3$, ppm): 152.7; EA Calc. for $C_{12}H_{18}OPBr$: C, 49.85; H, 6.27; Br, 27.63. Found: C, 50.42; H, 6.72; Br, 27.24%.

9.1.7. 2-I-phenyl-O-(diphenylphosphinite)

^{1}H NMR ($CDCl_3$, ppm): 6.70 (1H, t $^3J_{HH} = 7.2$ Hz), 7.07 (1H, d $^3J_{HH} = 8.4$ Hz), 7.16 (1H, t $^3J_{HH} = 7.2$ Hz), 7.35 (6H, m), 7.66 (4H, m), 7.73 (1H, d $^3J_{HH} = 8.4$ Hz); ^{13}C NMR ($CDCl_3$, ppm): 89.18 (d $J_{CP} = 2.2$ Hz), 117.7 (d $J_{CP} = 19.8$ Hz), 124 (s), 128.4 (d $J_{CP} = 7.3$ Hz), 129.35 (s), 129.87 (s), 130.33 (s), 130.7 (d $J_{CP} = 22.7$ Hz), 131.72 (d $J_{CP} = 24.9$ Hz), 139.41 (s), 140.32 (d $J_{CP} = 17.6$ Hz), 156.25 (d $J_{CP} = 9.5$ Hz); ^{31}P NMR ($CDCl_3$, ppm): 113.2; EA Calc. for $C_{18}H_{14}OPI$: C, 53.49; H, 3.49; P, 7.66. Found: C, 53.27; H, 3.31; P, 7.85%.

9.2. Complexation with bis-phosphinites

9.2.1. General procedure

58.3 mg (0.139 mmol; 1 equiv.) of Biphen($PiPr_2$)$_2$ and 50 mg (0.0695 mmol; 1 equiv. Rh) of $[Rh(COE)_2Cl]_2$ are dissolved in 5 mL dichloromethane (orange solution) and it was stirred over night at room temperature. The next day the solvent was removed in vacuo and the residing solid was dissolved in 2 mL of toluene which then was removed in vacuo again. The residing yellow brown solid was washed with 1 mL of pentane and dried in vacuo (yield: 70 mg, 90%).

9.2.1.1. [Biphen($OPiPr_2$)$_2$RhCl]$_2$. ^{1}H NMR ($CDCl_3$, ppm): 0.87 (6H, br m), 1.11 (6H, br m), 1.39 (12H, m), 1.99 (2H, br m), 2.62 (2H, br m), 7.07 (2H, br t), 7.14 (2H, br d), 7.19 (2H, br d), 7.24 (2H, br t); ^{13}C NMR ($CDCl_3$, ppm): 18.03 (s), 18.79 (d $J_{CP} = 3.9$ Hz), 19.14 (s), 19.32 (s), 19.91 (s), 20.15 (s), 34.85 (m), 121.82 (br s), 123.46 (s), 129.15 (d $J_{CP} = 9.9$ Hz), 131.37 (d $J_{CP} = 8.3$ Hz), 131.78 (s), 131.84; ^{31}P NMR ($CDCl_3$, ppm): 179.3 ($^1J_{RhP} = 229.8$ Hz), 180.4 ($^1J_{RhP} = 229.7$ Hz); EA Calc. for $C_{24}H_{36}RhO_2P_2Cl_2$: C, 51.77; H, 6.52; P, 11.12. Found: C, 51.32; H, 6.50; P, 11.82%.

9.2.1.2. [Biphen($OPCy_2$)$_2$RhCl]$_2$. ^{1}H NMR ($CDCl_3$, ppm): 1.0–2.4 (40H, m), 2.75 (4H, br s), 7.02 (1H, t $^3J_{HH} = 7.2$ Hz), 7.09 (1H, t $^3J_{HH} = 7.2$ Hz), 7.18 (4H, t $^3J_{HH} = 7.2$ Hz), 7.35 (4H, d $^3J_{HH} = 7.2$ Hz), 7.42 (4H, d $^3J_{HH} = 7.2$ Hz), 7.48 (2H, d $^3J_{HH} = 7.2$ Hz); ^{13}C NMR ($CDCl_3$, ppm): 25.4–30.3 (several br s), 45.72 (br m), 46.51 (br m), 117.82 (s), 121.99 (s), 123.34 (s), 128.92 (s)130.25 (s), 131.82 (br m), 132.22 (s), 154.62 (br d, $J_{CP} = 11.6$ Hz), 155.14 (s); ^{31}P NMR ($CDCl_3$, ppm): 180 (br s).

9.2.1.3. Crystal-structure analysis of [Biphen($OPCy_2$)$_2$-RhCl]$_2$. $C_{72}H_{104}Cl_2O_4P_4Rh_2 \cdot 4(C_6D_6)$, $M_r = 1770.63$, yellow fragment ($0.08 \times 0.12 \times 0.19$ mm^3), monoclinic, $I2/a$ (No.: 15), $a = 28.5238(3)$, $b = 10.5768(1)$, $c = 29.6343(3)$ Å, $\beta = 101.912(1)°$, $V = 8747.9(2)$ Å^3, $Z = 4$, $d_{calc} = 1.344$ g cm^{-3}, $F_{000} = 3680$, $\mu = 0.562$ mm^{-1}. Preliminary examination and data collection were carried out on an area diffraction system (Xcalibur™3, κ-CCD, OXFORD DIFFRACTIONS) and graphite monochromated Mo Kα radiation ($\lambda = 0.71073$ Å; sealed tube). Data collection were performed at 150 K within the Θ range of $2.81° < \Theta < 25.36°$. After merging ($R_{sig} = 0.0135$), 7991

[6792: $I_o > 2\sigma(I_o)$] independent reflections remained and all were used to refine 487 parameters. The structure was solved by a combination of direct methods and difference-Fourier syntheses. All non-hydrogen atoms were refined with anisotropic displacement parameters. All hydrogen atoms were placed in calculated positions and refined using a riding model. Full-matrix least-squares refinements were carried out by minimizing $\sum w(F_o^2 - F_c^2)^2$ and converged with $R_1 = 0.0303$ [$I_o > 2\sigma(I_o)$], $wR_2 = 0.0780$ [all data], GOF = 1.189, and shift/error <0.001. The final difference-Fourier map shows no striking features ($\Delta e_{min/max} = +0.63/-0.46$ e Å^{-3}). The target molecule [Biphen(OPCy$_2$)$_2$RhCl]$_2$ shows a crystallographic C_2 symmetry with an operator to equivalent atoms of (1/2 − x, y, −z) [7].

9.2.1.4. [Cy-1,2-CH$_2$-(OPPh$_2$)$_2$RhCl]$_2$. ^{1}H NMR ($CDCl_3$, ppm): 1.14–1.69 (10H, m), 3.46 (4H, br t), 4.12 (4H, dd $^2J_{HH} = 10.2$ Hz $^3J_{PH} = 25.9$ Hz), 7.00–7.08 (4H, m), 7.14 (6H, m), 7.22 (6H, m), 7.76 (4H, m); ^{13}C NMR ($CDCl_3$, ppm): 14.18 (s), 22.70 (s), 26.88 (s), 31.24 (d $J_{CP} = 4.5$ Hz), 43.57 (d $J_{CP} = 13.5$ Hz), 73.15 (d $J_{CP} = 13.6$ Hz), 127.43 (m), 128.92 (d $J_{CP} = 18.9$ Hz), 129.92 (d $J_{CP} = 10.9$ Hz), 131.16 (m), 131.72 (m), 133.42 (m), 133.70 (m); ^{31}P NMR ($CDCl_3$, ppm): 134.8 ($^1J_{RhP} = 225.8$ Hz), 134.9 ($^1J_{RhP} = 225.9$ Hz); EA Calc. for $C_{32}H_{34}RhO_2P_2Cl$: C, 59.05; H, 5.26; P, 9.52. Found: C, 58.94; H, 5.14; P, 9.89%.

9.2.1.5. Crystal-structure analysis of [Cy-1,2-CH$_2$-(OPPh$_2$)$_2$RhCl]$_2$. $C_{64}H_{68}Cl_2O_4P_4Rh_2 \cdot 2(CH_2Cl_2)$, $M_r = 1471.64$, yellow fragment ($0.20 \times 0.25 \times 0.64$ mm^3), monoclinic, $P2_1/c$ (No.: 14), $a = 8.7952(1)$, $b = 23.0017(2)$, $c = 16.1431(1)$ Å, $\beta = 93.3354(3)°$, $V = 3260.29(5)$ Å^3, $Z = 2$, $d_{calc} = 1.499$ g cm^{-3}, $F_{000} = 1504$, $\mu = 0.897$ mm^{-1}. Preliminary examination and data collection were carried out on a κ-CCD device (NONIUS, MACH3) with an Oxford Cryosystems cooling system at the window of a rotating anode (NONIUS FR591) with graphite monochromated Mo Kα radiation ($\lambda = 0.71073$ Å). Data collection were performed at 123 K within the Θ range of $2.18° < \Theta < 25.37°$. A total of 28031 intensities were integrated. Raw data were corrected for Lorentz, polarization, and, arising from the scaling procedure, for latent decay and absorption effects. After merging ($R_{sig} = 0.0176$), 5982 [5527: $I_o > 2\sigma(I_o)$] independent reflections remained and all were used to refine 514 parameters. The structure was solved by a combination of direct methods and difference-Fourier syntheses. All non-hydrogen atoms were refined with anisotropic displacement parameters. All hydrogen atoms were placed in calculated positions and refined using a riding model. Full-matrix least-squares refinements were carried out by minimizing $\sum w(F_o^2 - F_c^2)^2$ and converged with $R_1 = 0.0235$ [$I_o > 2\sigma(I_o)$], $wR_2 = 0.0601$ [all data], GOF = 1.092, and shift/error <0.001. The final difference-Fourier map shows no striking features ($\Delta e_{min/max} = +0.47/-0.30$ e Å^{-3}). The target molecule [Cy-1,2-CH$_2$-(OPPh$_2$)$_2$RhCl]$_2$ shows a crystallographic C_i symmetry with an operator to equivalent atoms of (1 − x, 1 − y, −z) [7].

10. Complexation with mono-phosphinites

10.1. General procedure

One hundred and fifty milligrams (0.304 mmol, 1 equiv.) of [(COD)RhCl]$_2$ and 179.6 mg (0.621 mmol; 2.04 equiv.) of 2-Br-phenyl-*O*-(diisopropylphosphinite) are dissolved in 5 mL of dichloromethane and it was stirred for 30 min Then the solvent was removed in vacuo to receive a yellow solid which was washed with 3 mL of pentane and dried in vacuo (yield: 303 mg; 0.57 mmol; 92%).

10.1.1. (COD)Rh(Cl)(2-Br-phenyl-O-(diisopropylphosphinite))

^{1}H NMR ($CDCl_3$, ppm): 1.35 (3H, d $^3J_{HH} = 7.2$ Hz), 1.38 (3H, d $^3J_{HH} = 7.2$ Hz), 1.52 (3H, d $^3J_{HH} = 7.2$ Hz), 1.57 (3H, d $^3J_{HH} = 7.2$ Hz), 1.98 (4H, m), 2.25 (4H, m), 2.75 (2H, hept $^3J_{HH} = 7.2$ Hz), 3.75 (2H, br s), 5.48 (2H, br s); 6.96 (1H, t $^3J_{HH} = 7.2$ Hz), 7.31 (1H, t $^3J_{HH} = 7.2$ Hz), 7.54 (1H, d $^3J_{HH} = 7.2$ Hz), 7.68 (1H, d $^3J_{HH} = 7.2$ Hz); ^{13}C NMR ($CDCl_3$, ppm): 17.89 (s), 19.33 (d $J_{CP} = 3.9$ Hz), 28.08 (s), 30.45 (d $J_{CP} = 18.5$ Hz), 32.98 (d $J_{CP} = 2.9$ Hz), 70.05 (d $J_{CRh} = 13.6$ Hz), 108.07 (dd $J_{CRh} = 5.8$ Hz $J_{CP} = 12.4$ Hz), 114.42 (d $J_{CP} = 3.9$ Hz), 120.32 (d $J_{CP} = 4.9$ Hz), 124.15 (s), 128.09 (s), 133.63 (s), 151.82 (d $J_{CP} = 8.8$ Hz); ^{31}P NMR ($CDCl_3$, ppm): 164.5 ($^1J_{RhP} = 174.4$ Hz); EA Calc. for $C_{20}H_{30}RhOPBrCl$: C, 44.84; H, 5.64; P, 5.78. Found: C, 44.99; H, 5.61; P, 5.87%.

10.1.2. Crystal-structure analysis of (COD)Rh(Cl)(2-Br-phenyl-O-(diisopropylphosphinite))

$C_{20}H_{30}BrClOPRh$, $M_r = 535.67$, yellow fragment ($0.08 \times 0.12 \times 0.19$ mm^3), triclinic, $P\bar{1}$ (No.: 2), $a = 7.7636(1)$, $b = 10.6205(1)$, $c = 14.5641(2)$ Å, $\alpha = 103.1144(6)°$, $\beta = 104.4772(6)°$, $\gamma = 103.8815(6)°$, $V = 1074.92(2)$ Å^3, $Z = 2$, $d_{calc} = 1.655$ g cm^{-3}, $F_{000} = 540$, $\mu = 2.858$ mm^{-1}. Preliminary examination and data collection were carried out on a κ-CCD device (NONIUS, MACH3) at the window of a rotating anode (NONIUS FR591) with graphite monochromated Mo Kα radiation ($\lambda = 0.71073$ Å). Data collection were performed at 293 K within the Θ range of $1.52° < \Theta < 25.41°$. A total of 28031 intensities were integrated. Raw data were corrected for Lorentz, polarization, and, arising from the scaling procedure, for latent decay and absorption effects. After merging ($R_{sig} = 0.0244$), 3443 [3077: $I_o > 2\sigma(I_o)$] independent reflections remained and all were used to refine 230 parameters. The structure was solved by a combination of direct methods and difference-Fourier syntheses. All non-hydrogen atoms were refined with anisotropic displacement parameters. All hydrogen atoms were placed in calculated positions and refined using a riding model. Full-matrix least-squares refinements were carried out by minimizing $\sum w(F_o^2 -$

$F_c^2)^2$ and converged with $R_1 = 0.0408$ [$I_o > 2\sigma(I_o)$], $wR_2 = 0.0942$ [all data], GOF = 1.151, and shift/error <0.001. The final difference-Fourier map shows no striking features ($\Delta e_{min/max} = +0.80/-0.53$ e Å^{-3}) [7].

10.1.3. (COD)Rh(Cl)(2-Br-phenyl-O-(dicyclohexylphosphinite))

^{1}H NMR ($CDCl_3$, ppm): 1.3–2.55 (30H, several m), 3.82 (2H, br s), 5.48 (2H, br s), 6.95 (1H, t $^3J_{HH} = 7.2$ Hz), 7.31 (1H, t $^3J_{HH} = 7.2$ Hz), 7.54 (2H, br d $^3J_{HH} = 7.2$ Hz); ^{13}C NMR ($CDCl_3$, ppm): 25.26 (s), 26.08 (d $J_{CP} = 11.0$ Hz), 26.32 (d $J_{CP} = 12.4$ Hz), 27.11 (d $J_{CP} = 5.9$ Hz), 28.22 (s), 32.00 (s), 39.94 (d $J_{Cp} = 16.8$ Hz), 70.08 (d $J_{CRh} = 13.2$ Hz), 78.68 (d $J_{CRh} = 13.9$ Hz), 107.61 (dd $J_{CRh} = 5.8$ Hz $J_{CP} = 12.44$ Hz), 120.37 (s), 124.13 (s), 128.11 (s), 133.71 (s), 152.12 (d $J_{CP} = 8.8$ Hz); ^{31}P NMR ($CDCl_3$, ppm): 162.4 ($^1J_{RhP} = 174.6$ Hz); EA Calc. for $C_{26}H_{38}RhOPBrCl$: C, 50.71; H, 6.34; P, 5.03. Found: C, 50.67; H, 6.34; P, 5.4%.

10.1.4. Crystal-structure analysis of (COD)Rh(Cl)(2-Br-phenyl-O-(dicyclohexylphosphinite))

$C_{26}H_{38}BrClOPRh$, $M_r = 615.79$, yellow fragment ($0.10 \times 0.12 \times 0.14$ mm^3), monoclinic, $P2_1/n$ (No.: 14), $a = 8.5885(1)$, $b = 18.4416(2)$, $c = 16.9592(2)$ Å, $\beta = 92.5055(4)°$, $V = 2683.53(5)$ Å^3, $Z = 4$, $d_{calc} = 1.524$ g cm^{-3}, $F_{000} = 1256$, $\mu = 2.300$ mm^{-1}. Preliminary examination and data collection were carried out on a κ-CCD device (NONIUS, MACH3) at the window of a rotating anode (NONIUS FR591) with graphite monochromated Mo Kα radiation ($\lambda = 0.71073$ Å). Data collection were performed at 293 K within the Θ range of $1.63° < \Theta < 25.35°$. A total of 61 537 intensities were integrated. Raw data were corrected for Lorentz, polarization, and, arising from the scaling procedure, for latent decay and absorption effects. After merging ($R_{sig} = 0.0352$), 4926 [3974: $I_o > 2\sigma(I_o)$] independent reflections remained and all were used to refine 280 parameters. The structure was solved by a combination of direct methods and difference-Fourier syntheses. All non-hydrogen atoms were refined with anisotropic displacement parameters. All hydrogen atoms were placed in calculated positions and refined using a riding model. Full-matrix least-squares refinements were carried out by minimizing $\sum w(F_o^2 - F_c^2)^2$ and converged with $R_1 = 0.0426$ [$I_o > 2\sigma(I_o)$], $wR_2 = 0.0790$ [all data], GOF = 1.093, and shift/error <0.001. The final difference-Fourier map shows no striking features ($\Delta e_{min/max} = +0.53/-0.56$ e Å^{-3}) [7].

10.1.5. (COD)Rh(Cl)(2-Br-phenyl-O-(diphenylphosphinite))

^{1}H NMR ($CDCl_3$, ppm): 2.09 (4H, m), 2.32 (4H, br s), 3.57 (2H, br s), 5.62 (2H, br s), 6.96 (1H, t $^3J_{HH} = 7.2$ Hz), 7.19 (2H, t $^3J_{HH} = 7.2$ Hz), 7.43 (6H, br s), 7.52 (2H, d and d overlapp), 7.92 (4H, m); ^{13}C NMR ($CDCl_3$, ppm): 26.27 (s), 27.10 (d $J_{CP} = 11.0$ Hz), 27.20 (d $J_{CP} = 12.4$ Hz), 28.15 (d $J_{CP} = 1.5$ Hz), 29.25 (s), 33.01 (s), 40.94 (d $J_{CP} = 17.6$ Hz), 70.91 (d $J_{CRh} = 13.9$ Hz), 107.57 (dd $J_{CRh} = 5.9$ Hz $J_{CP} = 12.4$ Hz), 114.62 (s), 120.39 (d $J_{CP} = 5.1$ Hz), 124.12 (s), 128.10 (s), 133.71 (s), 152.05 (d $J_{CP} = 11.0$ Hz); ^{31}P NMR ($CDCl_3$, ppm): 125.3 ($^1J_{RhP} = 180.3$ Hz); FAB(MS): 601 (m^+, $C_{26}H_{26}OPClBrRh$), correct isotopic pattern.

10.1.6. (COD)Rh(Cl)(2-Br-benzyl-O-(diisopropylphosphinite))

^{1}H NMR ($CDCl_3$, ppm): 1.3–2.55 (19H, several m), 3.82 (2H, br s), 5.48 (2H, br s), 6.95 (1H, t $^3J_{HH} = 7.2$ Hz), 7.31 (1H, t $^3J_{HH} = 7.2$ Hz), 7.54 (2H, br d $^3J_{HH} = 7.2$ Hz); ^{13}C NMR ($CDCl_3$, ppm): 18.39 (s), 18.47 (d $J_{CP} = 5.1$ Hz), 27.82 (d $J_{CP} = 16.8$ Hz), 28.37 (s), 33.19 (s), 67.35 (d $J_{CRh} = 13.2$ Hz), 69.82 (d $J_{CRh} = 13.9$ Hz), 106.95 (d $J_{CRh} = 5.9$ Hz), 107.09 (d $J_{CRh} = 5.9$ Hz), 121.62 (s), 127.70 (d $J_{CP} = 9.5$ Hz), 129.25 (s), 132.53 (s), 136.85 (d $J_{CP} = 5.1$ Hz); ^{31}P NMR ($CDCl_3$, ppm): 158.6 ($^1J_{RhP} = 176.4$ Hz); EA Calc. for $C_{21}H_{32}RhOPBrCl$: C, 45.88; H, 5.87; P, 5.63; Rh, 18.72. Found: C, 45.86; H, 5.79; P, 5.45; Rh, 18.6%.

10.1.7. (COD)Rh(Cl)(2,4-difluoro-6-Br-phenyl-O-(diisopropylphosphinite))

^{1}H NMR ($CDCl_3$, ppm): 1.26 (6H, dd $^3J_{HH} = 7.4$ Hz $^3J_{PH} = 16.0$ Hz), 1.37 (6H, dd $^3J_{HH} = 7.4$ Hz $^3J_{PH} = 16.0$ Hz), 1.92 (2H, br s), 2.18-2.3 (6H, m), 2.73 (2H, dhept $^3J_{HH} = 7.4$ $^2J_{HP} = 15$ Hz), 3.91 (2H, br s), 5.29 (2H, br s), 6.77 (1H, br t $^3J_{HF} = 7.4$ Hz), 7.00 (1H, d $^3J_{HF} = 7.4$ Hz); ^{31}P NMR ($CDCl_3$, ppm): 175.9 (dd, $^1J_{RhP} = 174.3$ Hz, $^4J_{PF} = 14.7$ Hz); EA Calc. for $C_{20}H_{28}RhOPBrClF_2$: C, 42.02; H, 4.94; P, 5.42. Found: C, 42.35; H, 4.84; P, 5.62%.

10.1.8. Crystal-structure analysis of (COD)Rh(Cl)(2,4-difluoro-6-Br-phenyl-O-(diisopropylphosphinite))

$C_{20}H_{28}BrClF_2OPRh$, $M_r = 571.65$, yellow fragment ($0.13 \times 0.18 \times 0.19$ mm^3), monoclinic, $P2_1/n$ (No.: 14), $a = 8.2136(2)$, $b = 26.3662(6)$, $c = 10.7809(3)$ Å, $\beta = 106.5661(11)°$, $V = 2237.82(10)$ Å^3, $Z = 4$, $d_{calc} = 1.697$ g cm^{-3}, $F_{000} = 1144$, $\mu = 2.764$ mm^{-1}. Preliminary examination and data collection were carried out on a κ-CCD device (NONIUS, MACH3) at the window of a rotating anode (NONIUS FR591) with graphite monochromated Mo Kα radiation ($\lambda = 0.71073$ Å). Data collection were performed at 293 K within the Θ range of $1.54° < \Theta < 25.34°$. A total of 14420 intensities were integrated. Raw data were corrected for Lorentz, polarization, and, arising from the scaling procedure, for latent decay and absorption effects. After merging ($R_{sig} = 0.0585$), 3964 [2899: $I_o > 2\sigma(I_o)$] independent reflections remained and all were used to refine 248 parameters. The structure was solved by a combination of direct methods and difference-Fourier syntheses. All non-hydrogen atoms were refined with anisotropic displacement parameters. All hydrogen atoms were placed in calculated positions and refined using a riding model. Full-matrix least-squares refinements were carried out by minimizing $\sum w(F_o^2 - F_c^2)^2$ and converged with $R_1 = 0.0564$ [$I_o > 2\sigma(I_o)$],

$wR_2 = 0.1119$ [all data], GOF = 1.055, and shift/error <0.001. The final difference-Fourier map shows no striking features ($\Delta e_{min/max} = +0.82/-0.70$ e Å^{-3}) [7].

10.1.9. (COD)Ir(Cl)(2,4-difluoro-6-Br-phenyl-O-(diisopropylphosphinite))

^{1}H NMR ($CDCl_3$, ppm): 1.33 (6H, dd $^3J_{HH} = 7.3$ Hz $^3J_{PH} = 15.9$ Hz), 1.42 (6H, d $^3J_{HH} = 7.4$ Hz $^3J_{PH} = 14.7$ Hz), 1.66-1.81 (4H, m), 2.01–2.17 (4H, m), 2.95 (2H, hept $^3J_{HH} = 7.4$ Hz), 3.52 (2H, br s), 5.04 (2H, br s), 6.84 (1H, dt $^3J_{HF} = 11$ Hz $^4J_{HH} = 2.5$ Hz), 7.08 (1H, dd $^3J_{HF} = 7.3$ Hz $^4J_{HH} = 2.4$ Hz); ^{31}P NMR ($CDCl_3$, ppm): 146.3 ($^4J_{FP} = 3.9$ Hz); ^{19}F NMR ($CDCl_3$, ppm): −166.8 (s), −115.3 (s); FAB(MS): 661 (m^+, $C_{20}H_{28}OPBrF_2ClIr$), correct isotopic pattern.

10.1.10. Crystal-structure analysis of (COD)Ir(Cl)(2,4-F-2-Br-phenyl-O-(diisopropylphosphinite))

$C_{20}H_{28}BrClF_2IrOP$, $M_r = 660.96$, yellow fragment ($0.16 \times 0.16 \times 0.19$ mm^3), monoclinic, $P2_1/n$ (No.: 14), $a = 8.2059(1)$, $b = 26.3152(3)$, $c = 10.7887(1)$ Å, $\beta = 106.2761(5)°$, $V = 2236.34(4)$ Å^3, $Z = 4$, $d_{calc} = 1.963$ gcm^{-3}, $F_{000} = 1272$, $\mu = 7.972$ mm^{-1}. Preliminary examination and data collection were carried out on a κ-CCD device (NONIUS, MACH3) at the window of a rotating anode (NONIUS FR591) with graphite monochromated Mo Kα radiation ($\lambda = 0.71073$ Å). Data collection were performed at 293 *K* within the Θ range of $1.55° < \Theta < 25.38°$. A total of 55938 intensities were integrated. Raw data were corrected for Lorentz, polarization, and, arising from the scaling procedure, for latent decay and absorption effects. After merging ($R_{sig} = 0.0527$), 4096 [2978: $I_o > 2\sigma(I_o)$] independent reflections remained and all were used to refine 248 parameters. The structure was solved by a combination of direct methods and difference-Fourier syntheses. All non-hydrogen atoms were refined with anisotropic displacement parameters. All hydrogen atoms were placed in calculated positions and refined using a riding model. Full-matrix least-squares refinements were carried out by minimizing $\Sigma w(F_o^2 - F_c^2)^2$ and converged with $R_1 = 0.0431$ [$I_o > 2\sigma(I_o)$], $wR_2 = 0.0862$ [all data], GOF = 1.020, and shift/error <0.001. The final difference-Fourier map shows no striking features ($\Delta e_{min/max} = +1.27/-0.88$ e Å^{-3}) [7].

10.1.11. (COD)Ir(Cl)(2,6-Br-phenyl-O-(diisopropylphosphinite))

^{1}H NMR ($CDCl_3$, ppm): 1.33 (6H, dd $^3J_{HH} = 7.2$ Hz $^3J_{HP} = 18.0$ Hz), 1.43 (6H, dd $^3J_{HH} = 7.2$ Hz $^3J_{HP} = 12.0$ Hz), 1.52-1.66 (4H, m), 1.91 (4H, m), 3.10 (2H, br s), 3.14 (2H, dhept $^3J_{HH} = 7.2$ Hz $^2J_{PH} = 13.2$ Hz), 5.03 (2H, br s),6.75 (1H, $^3J_{HH} = 8.4$ Hz), 7.43 (2H, $^3J_{HH} = 8.4$ Hz); ^{13}C NMR ($CDCl_3$, ppm): 18.22 (s), 18.27 (s), 18.28 (s), 18.31 (s), 28.16 (d, $J_{CP} = 1.5$ Hz), 31.18 (d, $J_{CP} = 26.4$ Hz), 33.52 (s), 52.30 (s), 96.82 (d, $J_{CP} = 13.9$ Hz), 117.25 (s), 125.04 (s), 132.40 (s), 150.61 (d, $J_{CP} = 8.0$ Hz); ^{31}P NMR ($CDCl_3$, ppm): 134.3.

10.1.12. (COD)Ir(Cl)(2-Br-benzyl-O-(diisopropylphosphinite))

^{1}H NMR ($CDCl_3$, ppm): 1.19 (3H, d $^3J_{HH} = 7.4$ Hz), 1.23 (3H, d $^3J_{HH} = 7.4$ Hz), 1.24 (3H, d $^3J_{HH} = 7.4$ Hz), 1.28 (3H, d $^3J_{HH} = 7.4$ Hz), 1.54–1.70 (4H, m), 1.99–2.06 (4H, m), 2.64 (dhept $^3J_{HH} = 7.4$ Hz, $^2J_{PH} = 7.45$ Hz), 3.38 (2H, br s), 4.72 (2H, d $^3J_{PH} = 4.9$ Hz), 4.83 (2H, br s), 7.02 (1H, t $^3J_{HH} = 7.4$ Hz), 7.19 (1H, t $^3J_{HH} = 7.4$ Hz), 7.25 (1H, d $^3J_{HH} = 7.4$ Hz), 7.36 (1H, d $^3J_{HH} = 7.4$ Hz); ^{13}C NMR ($CDCl_3$, ppm): 18.00 (d $J_{CP} = 4.4$ Hz), 18.30 (s), 27.90 (s), 28.89 (s), 33.53 (d $J_{CP} = 3.7$ Hz), 52.90 (s), 67.23 (s), 95.54 (d $J_{CP} = 5.9$ Hz), 121.54 (s), 127.62 (d $J_{CP} = 5.9$ Hz), 129.19 (s), 132.43 (s), 136.75 (d $J_{CP} = 5.1$ Hz); ^{31}P NMR ($CDCl_3$, ppm): 131.6 (s); EA Calc. for $C_{21}H_{32}IrOPBrCl$: C, 39.47; H, 5.05; P, 4.85. Found: C, 39.86; H, 4.91; P, 5.02%.

10.1.13. Crystal-structure analysis of (COD)Ir(Cl)(2-Br-benzyl-O-(diisopropylphosphinite))

$C_{21}H_{32}BrClIrOP$, $M_r = 639.01$, yellow fragment ($0.09 \times 0.12 \times 0.14$ mm^3), monoclinic, $P2_1/n$ (No.: 14), $a = 7.4756(1)$, $b = 22.9235(4)$, $c = 13.6594(2)$ Å, $\beta = 105.708(1)°$, $V = 2253.35(6)$ Å^3, $Z = 4$, $d_{calc} = 1.884$ g cm^{-3}, $F_{000} = 1240$, $\mu = 7.896$ mm^{-1}. Preliminary examination and data collection were carried out on a κ-CCD device (NONIUS, MACH3) with an Oxford Cryosystems cooling system at the window of a rotating anode (NONIUS FR591) with graphite monochromated Mo Kα radiation ($\lambda = 0.71073$ Å). Data collection were performed at 173 K within the Θ range of $1.78° < \Theta < 25.39°$. A total of 54195 intensities were integrated. Raw data were corrected for Lorentz, polarization, and, arising from the scaling procedure, for latent decay and absorption effects. After merging ($R_{sig} = 0.0328$), 4124 [3505: $I_o > 2\sigma(I_o)$] independent reflections remained and all were used to refine 219 parameters. The structure was solved by a combination of direct methods and difference-Fourier syntheses. All non-hydrogen atoms were refined with anisotropic displacement parameters. All hydrogen atoms were placed in calculated positions and refined using a riding model. Full-matrix least-squares refinements were carried out by minimizing $\sum w(F_o^2 - F_c^2)^2$ and converged with $R_1 = 0.0471$ [$I_o > 2\sigma(I_o)$], $wR_2 = 0.0892$ [all data], GOF = 1.221, and shift/error <0.001. ($\Delta e_{min/max} = +1.56/-1.01$ e Å^{-3}). A disorder over two positions [0.649(4):0.351(4)] of the (2-Br-benzyl)-moiety could be resolved clearly [7].

10.1.14. (COD)Ir(H)(Cl)(2-Br-phenyl-O-(diisopropylphosphinite))

^{1}H NMR ($CDCl_3$, ppm): −16.44 (1H, d $^2J_{PH} = 13.5$ Hz), 1.0–1.6 (12H, m), 2.48 (2H, m), 2.62 (2H, m), 2.96 (2H, m), 3.52 (2H, hept $^3J_{HH} = 7.4$ Hz), 4.78 (1H, br s), 5.00 (1H, br s), 5.08 (1H, br s); 5.45 (1H, br s), 6.58 (1H, t $^3J_{HH} = 7.4$ Hz), 6.67 (1H, d $^3J_{HH} = 7.4$ Hz), 7.05 (1H, d $^3J_{HH} = 7.4$ Hz); ^{13}C NMR ($CDCl_3$, ppm): 16.15 (d $J_{CP} = 5.1$ Hz), 16.49 (d $J_{CP} = 5.9$ Hz), 17.96 (d $J_{CP} = 4.4$ Hz), 18.07 (s), 27.27 (s), 27.89 (s), 27.99 (s),

28.21 (s), 28.75 (s), 28.75 (s), 29.11 (s), 30.22 (d J_{CP} = 2.9 Hz), 31.72 (s), 33.52 (s), 82.08 (s), 90.78 (s), 94.68 (d J_{CP} = 9.5 Hz), 100.00 (d J_{CP} = 14.6 Hz), 105.2 (d J_{CP} = 13.9 Hz), 123.29 (s), 128.91 (s), 159.3 (d J_{CP} = 8.1 Hz); ^{31}P NMR ($CDCl_3$, ppm): 146.9 ($^1J_{HP}$ = 13.5 Hz); EA Calc. for $C_{20}H_{30}IrOPBrCl$: C, 38.43; H, 4.84; P, 4.96. Found: C, 38.46; H, 4.73; P, 4.99%.

10.1.15. Crystal-structure analysis of (COD)Ir(H)(Cl)-(2-Br-phenyl-O-(diisopropylphosphinite))

$C_{20}H_{30}BrClIrOP$, M_r = 624.98, light yellow fragment (0.11 × 0.16 × 0.24 mm^3), monoclinic, $P2_1/c$ (No.: 14), a = 15.0935(2), b = 9.2737(1), c = 15.1021(2) Å, β = 90.3042(5)°, V = 2113.85(5) Å^3, Z = 4, d_{calc} = 1.964 g cm^{-3}, F_{000} = 1208, μ = 8.414 mm^{-1}. Preliminary examination and data collection were carried out on a κ-CCD device (NONIUS, MACH3) at the window of a rotating anode (NONIUS FR591) with graphite monochromated Mo Kα radiation (λ = 0.71073 Å). Data collection were performed at 293 *K* within the Θ range of 1.35° < Θ < 25.36°. A total of 55938 intensities were integrated. Raw data were corrected for Lorentz, polarization, and, arising from the scaling procedure, for latent decay and absorption effects. After merging (R_{sig} = 0.0284), 3884 [3235: $I_o > 2\sigma(I_o)$] independent reflections remained and all were used to refine 227 parameters. The structure was solved by a combination of direct methods and difference-Fourier syntheses. All non-hydrogen atoms were refined with anisotropic displacement parameters. All hydrogen atoms were placed in calculated positions and refined using a riding model. Full-matrix least-squares refinements were carried out by minimizing $\sum w(F_o^2 - F_c^2)^2$ and converged with R_1 = 0.0286 [$I_o > 2\sigma(I_o)$], wR_2 = 0.0598 [all data], GOF = 1.083, and shift/error <0.009. The final difference-Fourier map shows no striking features ($\Delta e_{min/max}$ = +0.77/−0.73 e Å^{-3}). The hydrogen atom bound to the Ir atom could be located in the final difference Fourier map. The refinement with an isotropic displacement parameter converged with reasonable results [U_{11} = 0.08(2), Ir–H 1.45(7) Å, and Cl–Ir–H 161(2)°] [7].

11. Ring closure

11.1. General procedure

Three hundred and three milligrams (0.567 mmol; 1 equiv.) of (COD)Rh(Cl)(2-Br-phenyl-*O*-(diisopropylphosphinite)) is dissolved in 20 mL of diethyl ether. The solution was cooled with an acetone/dry ice bath. Slowly 0.87 mL (72 mg; 1.124 mmol; 2 equiv.) of a 1.3 molar solution of sec. BuLi in cyclohexane/hexane are added. It is allowed to warm to room temperature over night. The color changes from orange to deeply red. Then 1 mL of degased water is added at room temperature and it is stirred for 1 min. The ether phase is immediately separated via canula in a new flask containing $MgSO_4$. It is stirred in the new flask for 5 min and the red ether solution is transferred into a new flask via canula from which the solvent is removed in vacuo. A deeply red solid is obtained (yield: 130 mg; 0.31 mmol; 55%). In some cases only a red viscose oil was received. This material can be used for the further reactions, as well.

11.1.1. (COD)Rh(2-phenyl-O-(diisopropylphosphinite))

^{1}H NMR (C_6D_6, ppm): 0.97 (6H, dd $^3J_{HH}$ = 7.4 Hz $^3J_{HP}$ = 13.5 Hz), 1.11 (6H, dd $^3J_{HH}$ = 7.4 Hz $^3J_{HP}$ = 13.5 Hz), 1.88 (2H, m $^3J_{HH}$ = 7.4 Hz $^3J_{PH}$ = 13.5 Hz), 2.05 (2H, m), 2.17 (4H, m), 4.39 (2H, s), 5.69 (2H, s), 7.02 (1H, t $^3J_{HH}$ = 7.4 Hz), 7.12 (1H, t $^3J_{HH}$ = 7.4 Hz), 7.27 (1H, t $^3J_{HH}$ = 7.4 Hz), 7.42 (1H, t $^3J_{HH}$ = 7.4 Hz); ^{13}C NMR (C_6D_6, ppm): 17.30 (s), 17.85 (d J_{CP} = 6.6 Hz), 29.25 (d J_{CP} = 3.7), 29.32 (s), 29.46 (d J_{CP} = 3.7 Hz), 32.15 (s), 81.19 (d J_{CRh} = 7.3 Hz), 98.63 (dd J_{CP} = 7.3 Hz J_{CRh} = 10.2 Hz), 110.01 (d J_{CP} = 14.6 Hz), 120.86 (s), 126.76 (s), 136.70 (s), 148.94 (dd J_{CP} = 8.8 Hz J_{CRh} = 35.9 Hz), 168.66 (d J_{CP} = 14.6 Hz); ^{31}P NMR (C_6D_6, ppm): 188.2 ($^1J_{RhP}$ = 196.2 Hz); EA Calc. for $C_{20}H_{30}RhOP$: C, 57.15; H, 7.19; P, 7.37. Found: C, 57.32; H, 7.01; P, 7.96%.

11.1.2. Crystal-structure analysis of (COD)Rh(2-phenyl-O-(diisopropylphosphinite))

$C_{20}H_{30}ORh$, M_r = 420.32, red fragment (0.11 × 0.12 × 0.18 mm^3), triclinic, $P\bar{1}$ (No.: 2), a = 8.2636(2), b = 10.2594(2), c = 12.6656(4) Å, α = 71.5921(12)°, β = 80.1638(13), γ = 66.8633(11), V = 935.55(4) Å^3, Z = 2, d_{calc} = 1.492 gcm^{-3}, F_{000} = 436, μ = 1.001 mm^{-1}. Preliminary examination and data collection were carried out on a κ-CCD device (NONIUS, MACH3) with an Oxford Cryosystems cooling system at the window of a rotating anode (NONIUS FR591) with graphite monochromated Mo Kα radiation (λ = 0.71073 Å). Data collection were performed at 173 K within the Θ range of 1.70° < Θ < 24.78°. A total of 19745 intensities were integrated. Raw data were corrected for Lorentz, polarization, and, arising from the scaling procedure, for latent decay and absorption effects. After merging (R_{sig} = 0.0436), 3143 [2690: $I_o > 2\sigma(I_o)$] independent reflections remained and all were used to refine 212 parameters. The structure was solved by a combination of direct methods and difference-Fourier syntheses. All non-hydrogen atoms were refined with anisotropic displacement parameters. All hydrogen atoms were placed in calculated positions and refined using a riding model. Full-matrix least-squares refinements were carried out by minimizing $\Sigma w(F_o^2 - F_c^2)^2$ and converged with R_1 = 0.0372 [$I_o > 2\sigma(I_o)$], wR_2 = 0.0877 [all data], GOF = 1.020, and shift/error <0.001. The final difference-Fourier map shows no striking features ($\Delta e_{min/max}$ = +0.71/−0.53 e Å^{-3}) [7].

11.1.3. (COD)Rh(2-phenyl-O-(dicyclohexylphosphinite))

^{1}H NMR (C_6D_6, ppm): 1.0–2.3 (30H, several m), 4.50 (2H, br s), 5.71 (2H, br s), 7.03 (1H, t $^3J_{HH}$ = 7.2 Hz), 7.24 (1H, t $^3J_{HH}$ = 7.2 Hz), 7.32 (1H, br d $^3J_{HH}$ = 7.2 Hz), 7.48 (1H, d $^3J_{HH}$ = 7.2 Hz); ^{13}C NMR (C_6D_6, ppm): 26.44 (s), 26.75 (d J_{CP} = 10.2 Hz), 27.01 (s), 27.16 (d

$J_{CP} = 3.7$ Hz), 27.75 (s), 28.12 (d $J_{CP} = 5.9$ Hz), 29.39 (s), 32.18 (s), 38.89 (d J $_{CP} = 2.9$ Hz), 39.11 (d $J_{CP} = 2.9$ Hz), 98.29 (dd $J_{CP} = 7.3$ Hz $J_{CRh} = 10.3$ Hz), 110.99 (d $J_{CRh} = 14.6$ Hz), 120.82 (s), 126.75 (s), 136.69 (s), 149.15 (dd $J_{CP} = 8.8$ Hz $J_{CRh} = 35.9$ Hz); ^{31}P NMR (C_6D_6, ppm): 182.22 ($^1J_{RhP} = 196.2$ Hz); EA Calc. for $C_{26}H_{38}RhOP$: C, 62.40; H, 7.65; P, 6.19. Found: C, 62.55; H, 7.34; P, 6.51%.

11.1.4. (COD)Rh(2-phenyl-O-(diphenylphosphinite))

^{1}H NMR (C_6D_6, ppm): 2.15 (4H, m), 2.22 (4H, br s), 4.48 (2H, br s), 5.98 (2H, br s), 7.15 (6H, m), 7.19 (2H, t and t overlapp $^3J_{HH} = 7.2$ Hz), 7.43 (1H, d $^3J_{HH} = 7.4$ Hz), 7.62 (2H, d $^3J_{HH} = 7.4$ Hz), 7.84 (4H, m); ^{13}C NMR (C_6D_6, ppm): 29.53 (s), 31.44 (s), 84.49 (d $J_{CRh} = 6.6$ Hz), 101.22 (dd $J_{CP} = 7.4$ Hz $J_{CRh} = 18.3$), 112.05 (d $J_{CP} = 16.1$ Hz), 121.53 (s), 127.05 (s), 128.60 (d $J_{CP} = 9.5$ Hz), 130.68 (s), 131.05 (d $J_{CP} = 14.6$ Hz), 136.86 (s), 149.72 (dd $J_{CP} = 9.5$ Hz $J_{CRh} = 35.1$ Hz), 166.92 (d $J_{CP} = 18.3$ Hz); ^{31}P NMR (C_6D_6, ppm): 153.7 ($^1J_{RhP} = 206.1$ Hz).

11.1.5. (COD)Rh(2-benzyl-O-(diisopropylphosphinite))

^{1}H NMR (C_6D_6, ppm): 0.72 (6H, dd $^3J_{HH} = 7.4$ Hz $^3J_{HP} = 15.6$ Hz), 0.96 (6H, dd $^3J_{HH} = 7.4$ Hz $^3J_{HP} = 15.6$ Hz), 1.63 (2H, dhept $^3J_{HH} = 7.4$ Hz), 1.9–2.2 (8H, m), 4.24 (2H, br s), 4.83 (2H, d $^3J_{PH} = 32.0$ Hz), 5.06 (2H, br s), 6.91 (1H, d $^3J_{HH} = 7.4$ Hz), 7.16 (1H, t $^3J_{HH} = 7.4$ Hz), 7.72 (1H, d $^3J_{HH} = 7.4$ Hz); ^{13}C NMR (C_6D_6, ppm): 17.31 (s), 17.82 (d $J_{CP} = 6.8$ Hz), 28.64 (d $J_{CP} = 23.3$ Hz), 30.74 (s), 31.77 (s), 79.88 (dd $J_{CP} = 5.8$ Hz $J_{CRh} = 11.7$), 84.39 (d $J_{CRh} = 6.8$ Hz), 98.80 (dd $J_{CP} = 7.8$ Hz $J_{CRh} = 11.7$ Hz), 122.81 (s), 126.02 (s), 126.89 (s), 137.42 (s), 143.45 (d $J_{CP} = 9.7$ Hz), 167.75 (d $J_{CP} = 10.7$ Hz $J_{CRh} = 32.1$ Hz); ^{31}P NMR (C_6D_6, ppm): 148.2 ($^1J_{RhP} = 178.2$ Hz); FAB(MS): 434 (m^+, $C_{21}H_{32}OPRh$), correct isotopic pattern.

11.1.6. Crystal-structure analysis of (COD)Rh(2-benzyl-O-(diisopropylphosphinite))

$C_{21}H_{32}OPRh$, $M_r = 434.35$, red fragment ($0.12 \times 0.14 \times 0.16$ mm^3), monoclinic, $P2_1/n$ (No.: 14), $a = 17.5016(2)$, $b = 14.2038(1)$, $c = 18.0305(2)$ Å, $\beta = 114.0985(4)°$, $V = 4091.54(7)$ Å^3, $Z = 8$, $d_{calc} = 1.410$ g cm^{-3}, $F_{000} = 1808$, $\mu = 0.918$ mm^{-1}. Preliminary examination and data collection were carried out on a κ-CCD device (NONIUS, MACH3) at the window of a rotating anode (NONIUS FR591) with graphite monochromated Mo Kα radiation ($\lambda = 0.71073$ Å). Data collection were performed at 293 K within the Θ range of $1.37° < \Theta < 25.31°$. A total of 98 022 intensities were integrated. Raw data were corrected for Lorentz, polarization, and, arising from the scaling procedure, for latent decay and absorption effects. After merging ($R_{sig} = 0.0606$), 7456 [4854: $I_o > 2\sigma(I_o)$] independent reflections remained and all were used to refine 441 parameters. The structure was solved by a combination of direct methods and difference-Fourier syntheses. All non-hydrogen atoms were refined with anisotropic displacement parameters. All hydrogen atoms were placed in calculated positions and refined using a riding model. Full-matrix least-squares refinements were carried out by minimizing $\sum w(F_o^2 - F_c^2)^2$ and converged with $R_1 = 0.0538$ [$I_o > 2\sigma(I_o)$], $wR_2 = 0.0981$ [all data], GOF = 1.090, and shift/error <0.001. The final difference-Fourier map shows no striking features ($\Delta e_{min/max} = +0.37/-0.45$ e Å^{-3}). In the asymmetric unit we found two crystallographic independent molecules **A** and **B**. They differ only slightly in their geometric parameters. Data given in Table 2 refer to **A** [7].

11.1.7. (COD)Rh(2,4-difluoro-6-phenyl-O-(diisopropylphosphinite))

^{1}H NMR (C_6D_6, ppm): 0.92 (6H, dd ^{3}JHH = 7.4 Hz $^3J_{PH} = 14.6$ Hz), 1.12 (6H, dd $^3J_{HH} = 7.4$ Hz $^3J_{PH} = 14.6$ Hz), 1.7–2.3 (8H, m), 4.39 (2H, br s), 5.42 (2H, br s), 6.72 (1H, t $^3J_{HH} = 7.2$ Hz), 6.95 (1H, d $^3J_{HH} = 7.2$ Hz); ^{13}C NMR (C_6D_6, ppm): 17.10 (s), 17.68 (d $J_{CP} = 7.3$ Hz), 29.13 (s), 29.53 (d $J_{CP} = 18.3$ Hz), 31.93 (s), 82.49 (d $J_{CR}h = 7.3$ Hz), 99.62 (dd $J_{CP} = 7.3$ Hz $J_{CRh} = 10.3$ Hz), 101.24 (dd $J_{CP} = 22.0$ Hz $J_{CF} = 5.9$ Hz), 116.54 (dd $J_{CP} = 16.1$ Hz $J_{CF} = 3.7$), 153.52 (dd $J_{CP} = 10.2$ Hz $J_{CRh} = 38.1$ Hz), 158.27 (d $J_{CP} = 6.6$ Hz); ^{19}F NMR (C_6D_6, ppm): −129.0, −122.8; ^{31}P NMR (C_6D_6, ppm): 194.6 ($^1J_{RhP} = 192.2$ Hz); EA Calc. for $C_{20}H_{28}RhOPF_2$: C, 52.64; H, 6.18. Found: C, 52.98; H, 6.05%.

11.1.8. (COD)Ir(2,4-difluoro-6-phenyl-O-(diisopropylphosphinite))

^{1}H NMR (C_6D_6, ppm): 0.84 (6H, dd $^3J_{HH} = 7.4$ Hz $^3J_{PH} = 15.9$ Hz), 0.99 (6H, d $^3J_{HH} = 7.4$ Hz $^3J_{PH} = 15.9$ Hz), 1.39 (2H, m), 1.71–1.86 (4H, m), 2.00 (4H, m), 3.88 (2H, br s), 5.04 (2H, br s), 6.66 (1H, dt $^3J_{HF} = 11$ Hz $^4J_{HH} = 2.5$ Hz), 7.08 (1H, dd $^3J_{HF} = 7.3$ Hz $^4J_{HH} = 2.4$ Hz); ^{31}P NMR (C_6D_6, ppm): 175.6; ^{19}F NMR (C_6D_6, ppm): −122.6 (s), −128.6 (s); FAB(MS): 546 (m^+, $C_{20}H_{28}OPF_2Ir$), correct isotopic pattern.

11.1.9. (COD)Ir(2-phenyl-O-(diisopropylphosphinite))

^{1}H NMR (C6D6, ppm): 0.99 (6H, dd $^3J_{HH} = 7.4$ Hz $^3J_{HP} = 13.5$ Hz), 1.18 (6H, dd $^3J_{HH} = 7.4$ Hz $^3J_{HP} = 13.5$ Hz), 1.88 (2H, m $^3J_{HH} = 7.4$ Hz $^3J_{PH} = 13.5$ Hz), 2.05 (2H, m), 2.17 (4H, m), 3.98 (2H, s), 5.42 (2H, s), 6.73 (1H, t $^3J_{HH} = 7.4$ Hz), 7.12 (1H, t $^3J_{HH} = 7.4$ Hz), 7.42 (1H, d $^3J_{HH} = 7.4$ Hz), 7.48 (1H, d $^3J_{HH} = 7.4$ Hz); ^{13}C NMR (C_6D_6, ppm): 16.98 (s), 17.03 (s), 29.35 (s), 29.67 (s), 29.98 (s), 32.99 (s), 66.72 (s), 88.29 (d $J_{CP} = 12.4$ Hz), 104.95 (d $J_{CP} = 14.6$ Hz), 122.53 (s), 152.40 (d $J_{CP} = 6.6$ Hz), 166.02 (d, $J_{CP} = 13.2$ Hz); ^{31}P NMR (C_6D_6, ppm): 171.2; EA Calc. for $C_{20}H_{30}IrOP$: C, 47.13; H, 5.93; P, 6.08. Found: C, 47.48; H, 5.61; P, 6.35%.

11.1.10. (COD)Ir(2-benzyl-O-(diisopropylphosphinite))

^{1}H NMR (C_6D_6, ppm): 0.74 (6H, dd $^3J_{HH} = 7.4$ Hz $^3J_{HP} = 15.6$ Hz), 0.99 (6H, dd $^3J_{HH} = 7.4$ Hz $^3J_{HP} =$

15.6 Hz), 1.75 (2H, dhept $^3J_{HH} = 7.4$ Hz), 1.8-2.2 (8H, m), 3.65 (2H, br s), 4.83 (2H, br s), 4.87 (2H, d $^3J_{PH} = 18.4$ Hz), 6.91 (1H, d $^3J_{HH} = 7.4$ Hz), 7.16 (1H, t $^3J_{HH} = 7.4$ Hz), 7.24 (1H, t $^3J_{HH} = 7.4$ Hz), 7.74 (1H, d $^3J_{HH} = 7.4$ Hz); ^{13}C NMR (C_6D_6, ppm): 17.21 (s), 17.54 (d $J_{CP} = 6.8$ Hz), 28.43 (d $J_{CP} = 23.3$ Hz), 31.56 (s), 32.74 (s), 68.27 (s), 79.71 (s), 88.84 (d $J_{CP} = 13.2$ Hz), 123.34 (s), 136.46 (s), 143.54 (d $J_{CP} = 7.3$ Hz), 165.46 (d $J_{CP} = 11.0$ Hz); ^{31}P NMR (C_6D_6, ppm): 128.9; EA Calc. for $C_{21}H_{32}IrOP$: C, 48.16; H, 6.16; P, 5.91. Found: C, 48.61; H, 6.00; P, 6.12%.

11.1.11. Crystal-structure analysis of RhClBr(2-phenyl-O-(diphenylphosphinite))(Br-2-phenyl-O-(diphenylphosphinite))$_2$

$C_{54}H_{42}Br_4ClO_3P_3Rh$, $M_r = 1289.79$, yellow fragment ($0.12 \times 0.10 \times 0.19$ mm^3), triclinic, $P\bar{1}$ (No.: 2), $a = 10.8877(5)$, $b = 13.5255(7)$, $c = 18.6668(1)$ Å, $\alpha = 69.494(5)$, $\beta = 101.912(1)°$, $\chi = 72.434(4)$, $V = 2453.9(2)$ Å^3, $Z = 2$, $d_{calc} = 1.746$ g cm^{-3}, $F_{000} = 1274$, $\mu = 3.802$ mm^{-1}. Suitable single-crystals for the X-ray diffraction study were selected under perfluorinated ether and fixed on a glass capillary. Preliminary examination and data collection were carried out on an area detecting system and graphite monochromated Mo Kα radiation ($\lambda = 0.71073$ Å). The unit cell parameters were obtained by full-matrix least-squares refinements during the scaling procedure. Data collections were performed at low temperatures (Oxford Diffraction cooling device) on a Oxford Diffraction Xcalibur3 system, κ-CCD; sealed tube, Enhance X-ray Source, Spellman DF3; nine data sets in rotation scan modus with $\Delta\phi/\Delta\omega = 2.0°$; d$x = 50$; $T = 150$ K. Intensities were integrated and the raw data were corrected for Lorentz, polarization, and, arising from the scaling procedure for latent decay and absorption effects. The structures were solved by a combination of direct methods and difference Fourier syntheses. All non-hydrogen atoms were refined with anisotropic displacement parameters. The difference Fourier map indicates an under occupancy of all bromine positions and residual electron density peaks with shorter distances of about 0.2 Å to the bonding carbon atoms or the rhodium atom. The indicated mixed occupancy with chlorine was refined with free variables for all positions and refined to a ratio of 0.75:0.25 (Br_1/Cl_1 and Br_2/Cl_2), 0.63:0.37 (Br_4/Cl_4) and 0.38: 0.62 (Br_5/Cl_5), respectively. The structure solution shows an heavy atom bonded to the phenyl group coordinated to the rhodium atom. The bond distance of 1.77 Å also indicates a chlorine atom. The difference Fourier map shows an under occupancy for this position and a small residual electron density located about 1.0 Å to the bonding carbon atom. Therefore a mixed occupancy with hydrogen is assumed, refining to a ratio of 0.70:0.30 for Cl_3/H_{11}. There is no indication of a mixed occupancy with bromine in the Cl_3 position. All aromatic hydrogen atoms were placed in ideal positions and refined using a riding model, aromatic d_{C-H} distances of 0.95 Å and $U_{iso}(H) = 1.2U_{eq}(C)$. Full-matrix least-squares refinements were carried out by minimizing $\sum\omega(F_o^2 - F_c^2)^2$ with the SHELXL-97 weighting scheme and stopped at shift/err <0.003. The final residual electron density maps showed no remarkable features [7].

12. Calculations

The DFT calculations were performed using the program suite GAUSSIAN 03 [6]. All molecular geometries were fully optimized. Transition states were obtained using the OPT2 function implemented in the program suite and proven to be one-dimensional saddle points by frequency analysis. The DFT method used includes Becke's three parameter hybrid exchange functional in combination with the correlation functional of Perdew and Wang (B3PW91). Geometry calculations and frequency calculations were performed using the valence double-zeta LANL2DZ basis set.

Supplementary material

CCDC 656929, 656930, 656931, 656932, 656933, 656934, 656935, 656937 and 656938 contains the supplementary crystallographic data for [Biphen($OPCy_2$)$_2$RhCl]$_2$, (COD)-Rh(2-benzyl-O-(diisopropylphosphinite)), (COD)Rh(Cl)-(2-Br-phenyl-O-(diisopropylphosphinite)), (COD)Rh(Cl)-(2-Br-phenyl-O-(dicyclohexylphosphinite)), (COD)Ir(H)-(Cl)(2-Br-phenyl-O-(diisopropylphosphinite)), (COD) Ir(Cl)-(2,4-F-2-Br-phenyl-O-(diisopropylphosphinite)), (COD)Rh-(2-phenyl-O-(diisopropylphosphinite)), (COD)Rh(Cl)(2,4-difluoro-6-Br-phenyl-O-(diisopropylphosphinite)) and [Cy-1,2-CH_2-($OPPh_2$)$_2$RhCl]$_2$. These data can be obtained free of charge from The Cambridge Crystallographic Data Centre via www.ccdc.cam.ac.uk/data_request/cif, or from the Cambridge Crystallographic Data Centre, 12 Union Road, Cambridge CB2 1EZ, UK; fax: (+44) 1223-336-033; or e-mail: deposit@ccdc.cam.ac.uk.

Acknowledgements

This work was supported by the DFG (Ru519/3-2). K. R. thanks Prof. W.A. Herrmann for the ability to use the infrastructure of his chair. K.R. gratefully acknowledges the support of Stephan D. Hoffmann who did the X-ray analysis of RhClBr(2-phenyl-*O*-(diphenylphosphinite))-(Br-2-phenyl-*O*- (diphenylphosphinite))$_2$ and [Biphen-($OPCy_2$)$_2$RhCl]$_2$.

References

[1] (a) J.-M. Basset, C. Coperet, L. Lefort, B.M. Maunders, O. Maury, E. Le Roux, G. Saggio, S. Soignier, D. Soulivong, G.J. Sunley, M. Taoufik, J. Thivolle-Cazat, J. Am. Chem. Soc. 127 (2005) 8604;
(b) J.-M. Basset, C. Coperet, D. Soulivong, M. Taoufik, J. Thivolle-Cazat, Angew. Chem. 118 (2006) 6228;
(c) F. Blanc, C. Coperet, J. Thivolle-Cazat, J.-M. Basset, Angew. Chem. 118 (2006) 6347;

(d) E. Le Roux, M. Taoufik, C. Coperet, A. de Mallmann, J. Thivolle-Cazat, J.-M. Basset, B.M. Maunders, G.J. Sunley, Angew. Chem. 117 (2005) 6913.

[2] (a) J.A. Martinho Simoes, J.L. Beauchamp, Chem. Rev. 90 (1990) 629;
(b) W.D. Jones, F.J. Feher, J. Am. Chem. Soc. 106 (1984) 1650;
(c) J.J. Low, A. Goddard Jr., J. Am. Chem. Soc. 106 (1984) 8321;
(d) P.E.M. Siegbahn, M.R.A. Blomberg, J. Am. Chem. Soc. 114 (1992) 10548.

[3] (a) G. Ujaque, F. Maseras, O. Eisenstein, L. Liable-Sands, A.L. Rheingold, W. Yao, R.H. Crabtree, New J. Chem. (1998) 1493;
(b) Z. Lu, C.H. Jun, S.R. de Gala, M.P. Sigalas, O. Eisenstein, R.H. Crabtree, Organometallics 14 (1995) 1168;
(c) C.N. Iverson, W.D. Jones, Organometallics 20 (2001) 5745;
(d) X. Zhang, G.B. Carpenter, D.A. Sweigart, Organometallics 18 (1999) 4887;
(e) H. Schwager, S. Spyroudis, K.P.C. Vollhardt, J. Organomet. Chem. 382 (1990) 191;
(f) J.J. Eisch, A.M. Piotrowski, K.I. Han, C. Krüger, Y.H. Tsay, Organometallics 4 (1985) 224;
(g) T. Schaub, U. Radius, Chem. Eur. J. 11 (2005) 5024.

[4] (a) B. Rybtchinski, S. Oevers, M. Montag, A. Vigalok, H. Rozenberg, J.M.L. Martin, D. Milstein, J. Am. Chem. Soc. 123 (2001) 9064;
(b) A. Sundermann, O. Uzan, D. Milstein, J.L. Martin, J. Am. Chem. Soc. 122 (2000) 7095;
(c) M. Gozin, A. Weisman, Y. Ben-David, D. Milstein, Nature 364 (1993) 699;
(d) B. Rytchinski, A. Vigalok, Y. Ben-David, D. Milstein, J. Am. Chem. Soc. 118 (1996) 12406;
(e) S.-Y. Liou, M. Gozin, D. Milstein, J. Am. Chem. Soc. 117 (1995) 9774;
(f) A. Vigalok, B. Rybtchinski, L.J.W. Shimon, Y. Ben-David, D. Milstein, Organometallics 18 (1999) 895–905;
(g) A. Vigalok, D. Milstein, Organometallics 19 (2000) 2061;
(h) A. Vigalok, D. Milstein, Organometallics 19 (2000) 2341;
(i) H. Salem, Y. Ben-David, L.J.W. Shimon, D. Milstein, Organometallics 25 (2006) 2292.

[5] (a) G. Giordani, R.H. Crabtree, Inorg. Synth. 28 (1990) 88;
(b) J.L. Herde, J.C. Lambert, C.V. Senoff, Inorg. Synth. 15 (1974) 18;
(c) A. Van der Ent, A.L. Onderdelinden, R.A. Schunn, Inorg. Synth. 28 (1990) 90.

[6] GAUSSIAN 03, Revision B.01, M.J. Frisch, G.W. Trucks, H.B. Schlegel, G.E. Scuseria, M.A. Robb, J.R. Cheeseman, J.A. Montgomery, Jr., T. Vreven, K.N. Kudin, J.C. Burant, J.M. Millam, S.S. Iyengar, J. Tomasi, V. Barone, B. Mennucci, M. Cossi, G. Scalmani, N. Rega, G.A. Petersson, H. Nakatsuji, M. Hada, M. Ehara, K. Toyota, R. Fukuda, J. Hasegawa, M. Ishida, T. Nakajima, Y. Honda, O. Kitao, H. Nakai, M. Klene, X. Li, J.E. Knox, H.P. Hratchian, J.B. Cross, C. Adamo, J. Jaramillo, R. Gomperts, R.E. Stratmann, O. Yazyev, A.J. Austin, R. Cammi, C. Pomelli, J.W. Ochterski, P.Y. Ayala, K. Morokuma, G.A. Voth, P. Salvador, J.J. Dannenberg, V.G. Zakrzewski, S. Dapprich, A.D. Daniels, M.C. Strain, O. Farkas, D.K. Malick, A.D. Rabuck, K. Raghavachari, J.B. Foresman, J.V. Ortiz, Q. Cui, A.G. Baboul, S. Clifford, J. Cioslowski, B.B. Stefanov, G. Liu, A. Liashenko, P. Piskorz, I. Komaromi, R.L. Martin, D.J. Fox, T. Keith, M.A. Al-Laham, C.Y. Peng, A. Nanayakkara, M. Challacombe, P.M.W. Gill, B. Johnson, W. Chen, M.W. Wong, C. Gonzalez, J.A. Pople, Gaussian Inc., Pittsburgh PA, 2003.

[7] (a) Data Collection Software for Nonius κ-CCD Devices, Delft (The Netherlands), 2001;
(b) Z. Otwinowski, W. Minor, Method Enzymol. 276 (1997) 307ff;
(c) A. Altomare, G. Cascarano, C. Giacovazzo, A. Guagliardi, M.C. Burla, G. Polidori, M. Camalli, SIR92, J. Appl. Crystallogr. 27 (1994) 435;
(d) Wilson, A.J.C. (Ed.), International Tables for Crystallography, vol. C, Tables 6.1.1.4, 4.2.6.8, and 4.2.4.2, Kluwer Academic Publishers, Dordrecht (The Netherlands), 1992;
(e) Spek, A.L., PLATON, A Multipurpose Crystallographic Tool, Utrecht University, Utrecht (The Netherlands), 2001;
(f) Sheldrick, G.M., SHELXL-97, Universität Göttingen, Göttingen (Germany), 1998.